The Thesis Committee for Juan José Muñoz Zapata
certifies that this is the approved version of the following thesis:

Holocene Geologic Slip Rate for the Mission Creek Strand of the southern San Andreas fault, Indio Hills

Committee:

Whitney M. Behr, Supervisor

Mark Cloos

Joel P. Johnson

Holocene Geologic Slip Rate for the Mission Creek Strand of the southern San Andreas fault, Indio Hills

by

Juan José Muñoz Zapata,

Thesis

Presented to the Faculty of the Graduate School of

The University of Texas at Austin

in Partial Fulfillment

of the Requirements

for the Degree of

Master of Science in Geological Sciences

The University of Texas at Austin

August 2017

Para Fernando y Claudia

Acknowledgments

I'd like to thank my adviser Dr. Whitney Behr, for her extreme patience with me throughout this process. Your high expectations, diligence, and passion for the earth sciences will serve as a blueprint for building my career. Thanks to my committee member Dr. Mark Cloos for sharing his inspiring knowledge of California tectonics and love for the geosciences. Thanks to my other committee member Dr. Joel Johnson for his support and helpful discussions about the geomorphic implications of my field area. I'd also like to thank my collaborators- Peter Gold for his guidance and help on lab work, Rosemarie Fryer for her significant contribution of the U-Series data, and Dr. Warren Sharp for his help with the U-Series lab work at the Berkeley Geochronology Center. Thanks to Dr. Arjun Heimsath and the Arizona State University Cosmogenic Nuclide Laboratory for allowing me to use their facility for ^{10}Be sample processing and the Center for Accelerated Mass Spectrometry at Lawrence Livermore National Laboratories for producing the ^{10}Be data. Thanks to the faculty at UT, the Behr Research Group, and my amazing friends that I've acquired in Austin. Thanks to the Jackson School of Geosciences for providing off-campus research funds, the Geological Society of America for their generous student grant, and the Southern California Earthquake Center for funding this project. Thanks to Dr. George Davis and Dr. Tom Casadevall, whose knowledge and generosity have provided me amazing opportunities in the earth sciences. Finally, I'd like to thank my family and parents, Fernando Munoz and Claudia Zapata for their love and support- tu hijo te quiere mucho tambien.

JUAN JOSÉ MUÑOZ ZAPATA

The University of Texas at Austin

August 2017

Holocene Geologic Slip Rate for the Mission Creek Strand of the southern San Andreas fault, Indio Hills

Juan José Muñoz Zapata, M.S.Geo.Sci.
The University of Texas at Austin, 2017

Supervisors: Whitney M. Behr,

Slip on the southern San Andreas fault in the northwestern Coachella Valley in Southern California is partitioned among three fault strands: the Mission Creek, Garnet Hill, and Banning strands. The NW-striking Mission Creek strand extends from the Indio Hills into the San Bernardino Mountains, whereas the Banning and Garnet Hill strands strike W-NW and transfer slip into the San Gorgonio Pass region. Together, these three faults accommodate $\sim$ 20 mm/yr of right-lateral motion based on geodetic slip rate estimates. Determining which strand accommodates the majority of fault slip and how slip rates on these strands have varied over Quaternary timescales is critical to seismic hazard assessment for this region. Here I present a new Holocene geologic slip rate estimate from an offset alluvial fan complex along the Mission Creek fault at the Three Palms site in the Indio Hills. The correlation of offset fans precisely located from a satellite image,

confirmed by field mapping and B4 LiDAR indicates that the Three Palms fan complex is offset 50.0 $\pm$ 5.0 meters. U-series dating on pedogenic carbonate rinds collected at 25-100 cm depth within the deposit constrain the minimum depositional age to 3.49$\pm$ 0.92 ka (95% CI), yielding a maximum slip rate of 19.2 $\pm$ 2.0 mm/yr. Cosmogenic ^{10}Be surface exposure dating on boulders yields a scattered dataset with high apparent inheritance and a median age of 13.6 +6.9/-6.7 ka (1σ error). However, the minimum boulder age of 5.4 $\pm$ 1.0 ka (2σ error) was interpreted as the maximum depositional age for the fan. This age, along with the preferred offset of 50.0 meters, yields a minimum slip rate of 7.8 $\pm$ 0.8 mm/yr. We therefore estimate a Holocene geologic slip rate of 7-21 mm/yr, with a preferred rate of 9-14 mm/yr. This rate overlaps within error with a previously published late Pleistocene slip rate on the Mission Creek strand of 12-22 mm/yr calculated at Biskra Palms Oasis a few kilometers to the southeast.

Contents

Acknowledgments **v**

Abstract **vii**

List of Tables **xi**

List of Figures and Plates **xii**

1 Introduction 1

2 Geologic Setting 2

2.1 Overview of the San Andreas Fault System 2

2.2 The Southern San Andreas Fault System 9

2.3 Previous Geologic Slip Rate Measurements in the Northern Coachella Valley 14

3 The Three Palms Slip Rate Site 15

4 Offset Models 22

5 Geochronology 24

5.1 U-series Dating on Pedogenic Carbonate 24

5.2 Cosmogenic ^{10}Be Surface Exposure Dating 31

5.3 Geochronometer Consistency and Interpreted Depositional Age . . 41

6 Holocene Geologic Slip Rate 43

7 Discussion 44

7.1 Implications for Slip Partitioning in the Coachella Valley 44
7.2 Implications for Quaternary Dating of Arid Region Alluvial Fans . 46
8 Conclusion 48

References **48**

Vita **60**

List of Tables

1 Table for U-Series Analytical Data (pt.1) (Fryer, 2016) 26

2 Table for U-Series Analytical Data (pt.2) (Fryer, 2016) 27

3 Table for ^{10}Be Analytical Data (pt. 1) 39

4 Table for ^{10}Be Analytical Data (pt. 2) 40

List of Figures and Plates

1 Map of the southern San Andreas Fault System 5
2 Map of the Coachella Valley Segment of the southern San Andreas fault zone 13
3 Geologic Map of the Three Palms Field Area 16
4 Panoramas of Three Palms alluvial fan 18
5 Three Palms Fan Complex Air Photos 19
6 Present day LiDAR of the Three Palms fan 20
7 Reconstructed LiDAR of the Three Palms fan 21
8 U-Series Isochron 30
9 U-Series Average 31
10 ^{10}Be Sample PDFs 38
11 Slip Rate Figure 43

1 Introduction

The San Andreas fault is the primary structure within the plate boundary system between the North American and Pacific Plates. The fault system is wide and extends from the Eastern California Shear Zone to offshore fault zones southwest of the Pacific coastline. The southern San Andreas fault system is a stick-slip segment of the plate boundary (Keller et al., 1982; Weldon and Sieh, 1985; Sieh, 1986; Sieh and Williams, 1990); meaning that the majority of the displacement it undergoes is manifested in moderate to severe ($\geq$ M6.0) surface-rupturing events. Furthermore, this section of the fault system does not rupture frequently and has not in over 150 years, so there is uncertainty as to which fault zones and strands accommodate the majority of PAC-NA plate motion at this latitude over recent timescales, and consequently, which fault strands pose the greatest seismic risk to densely populated southern California communities. Geodetic techniques allow for real-time to very recent ($\sim$20 year) measurements (Fay and Humphreys, 2005; Spinler et al., 2010) of velocities in the southern San Andreas fault system. However, its resolution is limited both temporally and spatially. Geodetic techniques cannot capture fault slip behavior averaged over longer timescales or potential temporal variations. Although it can estimate rates averaged across several fault strands, it cannot resolve the rates of individual faults and their along-strike variations. Therefore, geologic slip rates, which are acquired from measuring the age of offset geomorphic features as well as quantifying their displacements, can provide time-averaged slip information on different structures, at different locations along strike, and averaged over different timescales (Keller et al., 1982; van der Woerd et al., 2006; Behr et al., 2010; Gold et al., 2015).

In this thesis, I present a newly discovered slip rate site along one of the several strands of the complex southern San Andreas fault in the Indio Hills in the Coachella Valley region. At this location, a Holocene alluvial fan complex is offset, and the offset features are documented to estimate the amount of displacement along the fan. Two different Quaternary geochronometers (U-series on pedogenic carbonates and cosmogenic ^{10}Be dating)

were used to constrain the age of the top of the fan. I use these measurements to calculate a Holocene geologic slip rate for the Mission Creek strand of the southern San Andreas fault. The result is compared to previously published estimates averaged over longer Pleistocene timescales ($\sim$50 ky) (Behr et al., 2010) I explore implications for spatial and temporal variations in fault slip rates along the southern San Andreas Fault zone in the Coachella Valley, as well as for quaternary geochronology of arid alluvial fans are also revisited in the discussion.

2 Geologic Setting

2.1 Overview of the San Andreas Fault System

The San Andreas Fault System is a large-scale continental transform fault that resolves the motions between the North American and Pacific Plates (Wallace, 1990; Kendrick, 2015). The present strike-slip motion of the fault system originated after the cessation of subduction of the Farallon plate under the North American plate, which began about 155 Ma (Atwater, 1970; Sigloch and Mihalynuk, 2013). Atwater, 1970 realized how the system evolved after Farallon subduction as follows: The cessation of subduction was evidenced by the south-down progression of ages of easternmost magnetic anomalies off of the California coast. The oldest one (29 Ma) is at the Mendocino Triple Junction in Northern California, and the youngest one (4 Ma) is off the coast of Southern California near Baja California. The plate reconstruction realized by Atwater, 1970 reveals the impingement of the ridge at 28 Ma. The fault system then had two different rates of motion as it developed along the California coast. The northern triple junction moved consistently and focused the majority of the plate motion on the linear San Andreas fault zone. The southern triple junction (RTF), which is an inherently different triple junction than the northern one (FFT), moved consistently until it started nearing the latitude of Baja California, where there is a ridge. This study showed the evolution of the southern ridge-trench-fault triple junction, which

caused the uplift of the Transverse Ranges and the structurally complex San Gorgonio Pass. It also determined that the San Andreas fault system, in its modern form, is around 4-5 m.y. old (Atwater, 1970).

The most prominent structure within the San Andreas Fault System is the San Andreas fault itself, which is a dominantly right-lateral strike-slip fault that runs in a northwest direction from Bombay Beach along the Salton Sea in southern California, takes a western bend in the Coachella Valley and continues northwest after passing through the San Gabriel mountains until it ends in offshore northern California at the Mendocino Triple Junction. The fault became widely recognized by the general public after the great San Francisco earthquake of 1906, which was officially reported by Andrew C. Lawson, who gave the fault its name in 1895 as the "San Andreas Rift" (Lawson and Reid, 1908; Wallace, 1970). The fault has since been studied by many geologists, including before (Willis, 1938; Gutenberg, 1941) and after the advent of plate tectonic theory, and it is currently recognized as a critical component of California's geologic history (Matti et al., 1992). One of the most significant early studies of the San Andreas fault was conducted by Mason Hill and Thomas Dibblee in 1953, who recognized that hundreds of miles of lateral movement had been accommodated by this structure (Hill and Dibblee, 1953).

At its full extent, the San Andreas fault is 1300 km long (Hill and Dibblee, 1953; Wallace, 1970) and can be divided into four main sections. The northernmost section of the fault extends from just east of Monterey, CA, to its northern limit at the Mendocino Triple Junction. The majority of this northern section is continuous and locked, and it includes an array of auxiliary faults in the surrounding fault zone, including various splays in the San Francisco Bay Area. It has a long-recorded history of rupture events near San Francisco, including the M7.8 1906 San Francisco earthquake and the M6.9 1989 Loma Prieta earthquake. The northern central section runs continuously northwest for about 100 km between Parkfield and San Juan Bautista, CA. Although there have been a cluster of M5.5-6.0 earthquakes near Parkfield, CA in recent history, the fault north of this city is

creeping (<M7.0), with no large recorded seismic activity. The south-central section is located between the San Gabriel Mountains and Parkfield, CA; this is a continuous and locked section that last had a major rupture in 1857 during the M7.9 Fort Tejon earthquake. The southern section of the San Andreas fault, which extends from the inception of the fault at Bombay Beach along the Salton Sea to the San Gabriel Mountains, is a very complex and discontinuous locked section that includes a western 'Big Bend' in the San Andreas fault that begins at San Gorgonio pass in the northern Coachella Valley and defines the E-W-striking Transverse Ranges that dominate southern California topography.

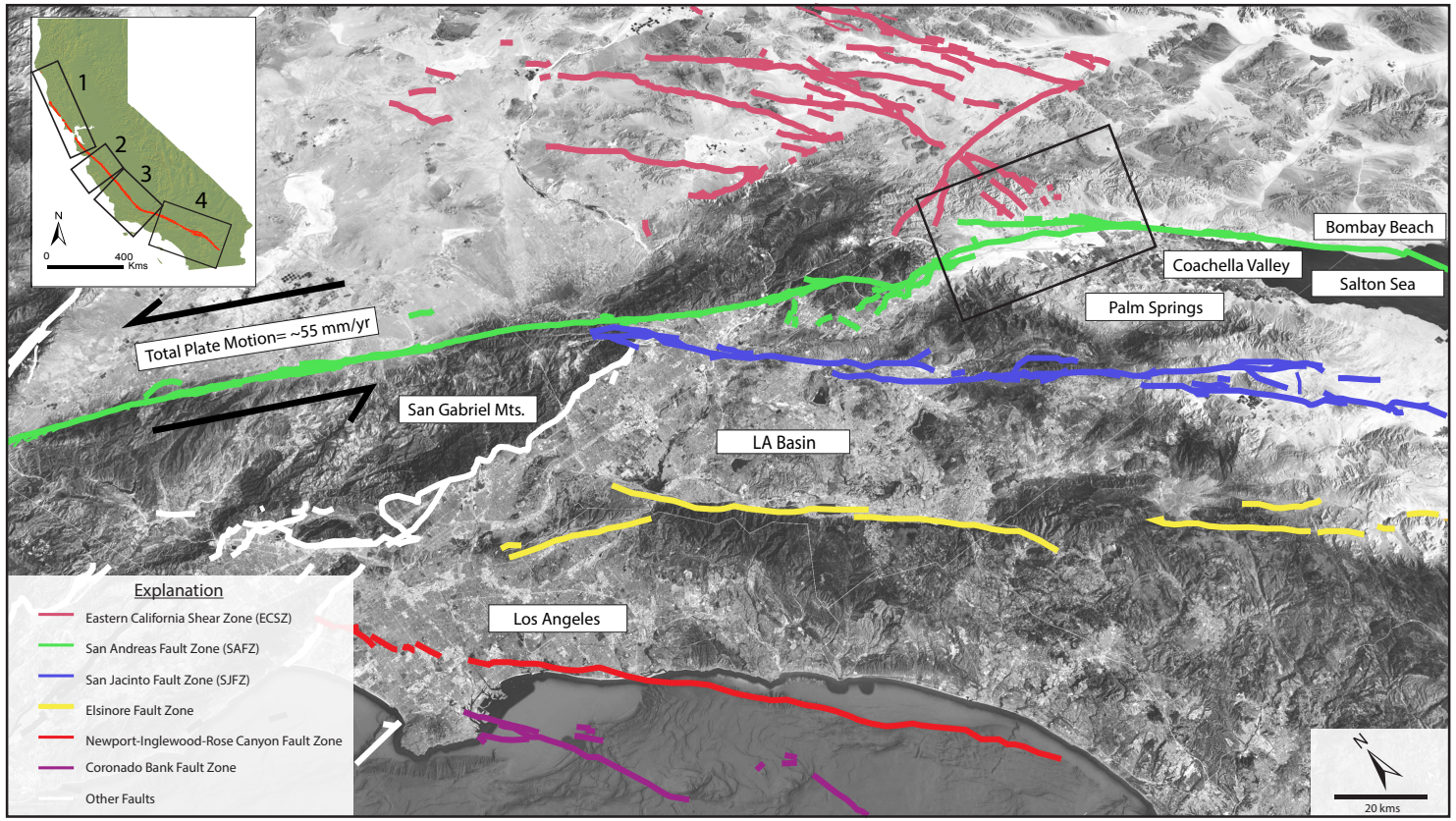

Figure 1: Overview oblique black and white in map of southern California and of the southern San Andreas fault system, which includes several fault zones that accommodate slip between the Pacific and North American Plates. Diagonal black rectangle toward the upper right of the figure highlights the Coachella Valley section of the southern San Andreas fault zone (Seen in Figure 2). Total slip between all of the fault is ~55 yr. Imagery from Google Earth. Quaternary faults from USGS.

There has been a long history of trying to quantify the present-day rates of motion between the Pacific and North American plates and along the numerous faults within the San Andreas Fault System beginning from Atwater, 1970. Early work by (Minster and Jordan, 1978) determined from a circumglobal dataset that the Pacific-North American (PA-NA) plate boundary accommodates around 56 mm/yr of plate motion. One of the first plate motion models constrained by GPS (NUVEL-1A) predicted a relative PA-NA velocity of 54.6 $\pm$ 2.3 mm/yr, while a more recent geodetic model (MORVEL) predicts 50.2 $\pm$ 1.1 mm/yr (Argus and Gordon, 1991; DeMets et al., 2010). Based on these plate motion models, the velocity between the Pacific and North American plates is well constrained. In many places along the northern section of the San Andreas fault, the fault zone and fault system is confined to a small array of faults that are adjacent to the main break, so most of the plate motion is accommodated by the San Andreas fault zone itself. In southern California, however, the plate boundary is a fault system that is much wider, and the $\sim$50 mm/yr of displacement is distributed among several different fault zones extending from the continental borderland to the eastern Mojave desert. In these regions where the San Andreas System is distributed, geodesists commonly invert their data and use block models to examine the ways in which total PAC-NA plate motion is partitioned among individual structures (Fay and Humphreys, 2005; Fialko, 2006; Spinler et al., 2010). I discuss this in more detail for the southern San Andreas fault system in Section 2.2.

In addition to geodetic constraints on slip rates, geologic measurements of fault slip rates provide complementary data at greater spatial resolution but averaged over longer timescales. Geologic slip rates rely on offset geomorphic features, most often offset alluvial fans (Keller et al., 1982; Kirby et al., 2006; Oskin et al., 2007; Behr et al., 2010; Gold et al., 2015), stream channel thalwegs (Wesnousky et al., 1991; Frankel et al., 2007b; Blisniuk et al., 2010), and fluvial terrace risers (Kirby et al., 2006; Cowgill, 2007; Blisniuk et al., 2010). The offset amounts are commonly determined using detailed geomorphic analysis from high-resolution topographic data. The depositional or surface stabilization ages

are determined using Quaternary geochronometers such as radiocarbon, cosmogenic ^{10}Be surface exposure, U-Series on pedogenic carbonate, Optically Stimulated Luminescence (OSL), and others. The acquisition of high resolution airborne Light Detection and Ranging (LiDAR) data for the entire San Andreas fault and several adjacent fault zones in the mid-2000's has led to a proliferation in fault slip rate studies, especially in well-exposed arid regions of southern California. In some areas, these data suggest good correlations between geologic slip rates and block models based on inversions of geodetically-constrained horizontal velocities, indicating constancy of seismic strain release over timescales as long as the Late Pleistocene to the last decades (Blisniuk et al., 2012). Good correlations occur when the block models based on geodetic data match the geologic slip rate determined for a section of the fault at that latitude within reasonable error depending on the time scale. In the southern San Andreas fault alone, there have been multiple (5+) studies that have used geodetic data to produce block models that attempt to constrain recent ($\sim$20 year) slip rates, e.g. (Becker et al., 2005; Fay and Humphreys, 2005; Fialko, 2006; Spinler et al., 2010; Lindsey and Fialko, 2013). Of these studies, most of the models produced yield rates that compare relatively well with geologic slip rate estimates. However, apparent discrepancies of up to 10 mm/yr between geologic and geodetic slip rates for this region have also been recorded in other studies (Dorsey, 2003; van der Woerd et al., 2006). Other regions such as the Eastern California Shear Zone show significant discrepancies between geologic slip rates and block models based on inversions of geodetically-constrained horizontal velocities, suggesting slip rates vary over time due to changes in fault loading at shorter time and spatial scales than plate boundary loading rates (Kirby et al., 2006; Frankel et al., 2007b). In previous studies, slip rate discrepancies between geologic and geodetically constrained block models have largely been attributed to uncertainties in geologic measurements, such as the 15 mm/yr discrepancy found in the Altyn Tagh fault in Mongolia (Bendick et al., 2000; Cowgill, 2007; Cowgill et al., 2009). Comparing and reconciling these rates gives us an idea of how often seismic strain is released and consequently, how often surface ruptur-

ing (M6.0+) seismic events occur in a given region. However, this cannot be quantifiably determined, as this strain could have been released in many different events, with varying degrees of magnitude, over different locations along strike.

Another type of analysis that complements present-day plate and fault motion rates from geodesy and long term time-averaged slip rates from geology, focuses on quantifying earthquake rupture histories and recurrence intervals for faults in the San Andreas System over thousand-year timescales. This documentation comes from both historical records (e.g. Franciscan Missions, Gold Rush Era newspaper clippings), and paleoseismic studies, which involve detailed interrogation of subsurface stratigraphy adjacent to faults. Paleoseismology was pioneered by Kerry Sieh in 1974 and has greatly improved the temporal resolution and timespan of California earthquake records. In the northern section of the San Andreas fault, the last major surface rupturing event near a highly-populated area occurred in 1906, more than a century ago. Since then, smaller events have occurred, like the M7.3 1980 Eureka earthquake (which happened in a remote area of Northern California, no casualties and a minor economic impact) and the disastrous M6.9 1989 Loma Prieta earthquake. Long-term paleoseismic records suggest that the earthquake recurrence interval in this section on average is 95-110 years (Field, 2007). However, paleoseismic data from the region indicate that there has only been one major surface rupture event (1906 San Francisco Earthquake) in the last 340 years (Schwartz et al., 1998). Since the north-central section experiences aseismic creep, there haven't been any major recorded seismic events, although it is unclear if there have been any unrecorded events. However, the intersection between the north-central creeping section and the south-central section of the fault, located at the small community of Parkfield, has experienced a magnitude 6 or greater earthquake every $\sim$22 years since the mid 1800's, except for the last event, which occurred 15 years late (Langbein et al., 2005). On the south-central section, the last major surface rupturing event was the M7.9 1857 Fort Tejon earthquake, 160 years ago. Paleoseismic studies conducted in the Carrizo plain show an fault slip recurrence interval of 140 $\pm$ 36 years for fault slip

events of M6.0 or higher, given that other smaller events most likely could have occurred between this recurrence interval (Zielke et al., 2010).

In summary, the San Andreas fault system is a complex plate boundary with uncertain slip rate parameters across the different fault zones that compose it. The development of new tools enhance understanding of the local rates of motion and earthquake rupture history throughout California. Although an abundance of data have been collected over the last 100 years, there are still many questions surrounding the finer details of the fault system, especially in complex regions. Among the most complex regions is the Big Bend region within southern California, which will be the focus of the next section.

2.2 The Southern San Andreas Fault System

The southern San Andreas fault system is part of the greater San Andreas Fault System that extends from its inception at Bombay Beach in the Salton Sea to the southeastern San Gabriel mountains just north of Los Angeles. In this area perpendicular to the strike of the San Andreas fault proper, the fault system here is around 400 km wide, extending from the continental borderland in the west to the Mojave desert in the east. The system includes the following major fault zones (starting from the southwest, going to the northeast): San Clemente, Elsinore, San Jacinto, San Andreas, and Eastern California Shear Zone (ECSZ). Several geodetic block models constrain short-term slip rates for these fault zones, although published rate estimates vary as a function of model input parameters and assumptions such as lithospheric viscosity and thickness, locking depth, number and geometry of the blocks, fault geometries, and influence of minor structures (Sauber et al., 1994; Becker et al., 2005; Fay and Humphreys, 2005; Fialko, 2006; Spinler et al., 2010). Generally, geodetic rates appear to be fastest along the San Andreas (20-23 mm/yr) (Spinler et al., 2010) and San Jacinto (12 mm/yr) (Spinler et al., 2010) Fault zones, and are slower along the Elsinore (3 to 4 mm/yr) (Becker et al., 2005) and ECSZ (0.6- 1.3 mm/yr over individual faults) (Amos et al., 2013).

In this section, on the southern San Andreas fault itself, the following nomenclature will be applied. The terms segment, strand, and splay are used in a hierarchical fashion, where a segment represents a regional domain of San Andreas fault strands, that may consist of two or more fault splays. The San Andreas fault zone northwest of the San Gorgonio pass region in the northern Coachella Valley is known as the San Bernardino strand of the Mojave segment, and the continuous 70 km section that runs from Bombay Beach to Biskra Palms Oasis the Indio strand of the Coachella Valley segment. In this study, I focus on the southern San Andreas fault zone southeast of San Gorgonio Pass, which includes the Garnet Hill, Banning, and Mission Creek strands of the Coachella Valley segment, following the usage of Allen (1957).

The Coachella Valley segment of the southern San Andreas Fault begins as a single continuous fault just east of the Salton Sea and extends about 70 km in a northwest direction to the western end of San Gorgonio Pass. At Biskra Palms Oasis just north of Indio, CA, the Indio strand of the Coachella Valley segment splits into two additional strands: the Mission Creek Fault and the Banning Fault. The dominantly right-lateral strike-slip Mission Creek strand, which strikes northwestward and bounds the northern Indio Hills, intersects northeast trending faults of the Eastern California Shear Zone (Pinto Mountain, Mill Creek Fault Zones) in the San Bernardino Mountains. The right-lateral oblique Banning fault, which bends more westerly, continues through the central Coachella Valley into the San Gorgonio Pass region. In the northwest Indio Hills near Edom Hill, the Banning Fault is interpreted to transfer slip onto the poorly understood, right-lateral oblique, Garnet Hill Fault (Yule and Sieh, 2003; Gold et al., 2015). Both the Banning and Garnet Hill faults continue toward the west where they merge into the San Gorgonio Pass Fault Zone in the northwest Coachella valley near Whitewater River. The San Gorgonio Pass fault zone is a 20-km-wide contractional stepover whose dominant structures are the San Gorgonio Pass-Garnet Hill faults which are dextral-reverse faults dip moderately northward (Yule and Sieh, 2003) that join the Coachella Valley segment of the southern San Andreas fault to the San

Bernardino segment of the Southern San Andreas fault zone at the western end of the San Gorgonio Pass.

The long term tectonic history of southern San Andreas fault strands is complex as there have been significant reorganizations over time. The Mission Creek strand is part of a paleotectonic system in the San Bernardino mountains that has generated 160 km of right lateral displacement, recording the entire history of the San Andreas fault in this area over the last 5 Ma (Matti and Morton, 1993; Gold et al., 2015). The reconstruction of the history of the southern San Andreas fault zone since about at about 6 Ma, when the abandonment of the San Gabriel-Banning fault produced 40 km of slip (Matti and Morton, 1993; Gold et al., 2015). The Mission Creek fault formed in Pliocene (3.5-4 Ma) time and produced an additional 89 km of slip that juxtaposed the San Gabriel Mountains block from the San Bernardino Mountains block (Matti and Morton, 1993; Gold et al., 2015). The Mission Creek strand was then deformed at 1.2 Ma because of a structural knot in the San Gorgonio Pass and was eventually abandoned in the late Pleistocene, passing the majority of displacement off to the newly initiated San Jacinto fault zone to the southwest at 1.2 Ma and then the Mill Creek fault to the northeast at 500 ka (Matti and Morton, 1993; Gold et al., 2015). After accommodating 8 km of displacement, the Mission Creek fault shifted again to the southwest at 125 ka and formed the neotectonic San Bernardino segment of the San Andreas fault, where it connects with the Banning fault which is on the western end of the Coachella Valley segment (Matti and Morton, 1993; Gold et al., 2015).

Along the southern San Andreas fault, there have been no recorded major (+M7.5) earthquakes. Paleoseismic studies on the Coachella Valley Segment, 10 km southeast of the Biskra Palms site indicate that the last major seismic event there occurred in A.D. 1676 ± 35 years (Sieh et al., 1989; Sieh and Williams, 1990). On the Mission Creek strand at Thousand Palms Oasis, there is evidence that indicates there were four or five surface rupturing events over the last 1200 years, with the earliest having occurred in A.D. 820 and the most recent having occurred in the range of A.D. 1520-1680 (which is reported in this study to be

more than likely the same as the A.D. 1676 $\pm$ 35 years event found in Sieh and Williams, 1990), (Fumal et al., 2002). An important conclusion from this study was the recurrence interval for surface rupturing earthquakes on the San Andreas fault in the Coachella Valley, which was found to be 215 $\pm$ 25 years for five events, whereas the elapsed time since the most recent event is 326 $\pm$ 35 years, which suggests the Coachella Valley segment of the southern San Andreas fault zone is likely near failure. Other paleoseismic studies on the San Andreas fault in the San Gorgonio pass indicate that there is evidence for a 300-year average recurrence interval, with five surface-rupturing events that are irregularly spaced from 100-475 years (Yule and Sieh, 2001).

Because of the long quiescence since the last major earthquake on the southern San Andreas fault, it is considered one of the most hazardous sections of the San Andreas System in southern California. Current scenario earthquake rupture models initiate ruptures at Bombay Beach, which propagate northwestward toward the Indio Hills and Biskra Palms then across the Northern Coachella Valley. However, the northwestward increase in complexity of the Coachella Valley segment of the southern San Andreas fault as it approaches San Gorgonio Pass has raised a number of intriguing questions regarding the seismic hazard potential of Coachella Valley fault strands to the densely populated Los Angeles Basin. For example, 1) Will an earthquake rupture generated on the Indio strand propagate along the Mission Creek fault toward the central San Bernardino Mountains, or along the Banning and/or Garnet Hill strand into the San Gorgonio Pass region? 2) If a rupture is concentrated on the Mission Creek strand, will it propagate through the San Bernardino Mountains into the Los Angeles Basin, or will slip be transferred onto intersecting faults in Eastern California Shear Zone? 3) If a slip is concentrated (awaiting rupture) on the Banning or Garnet Hill faults, will it propagate through the San Gorgonio Pass structural complexity? In lieu of a major earthquake, a primary method of answering these questions is to investigate how these faults have behaved in the past by documenting cumulative slip rates both with distance along strike, as well as over multiple timescales.

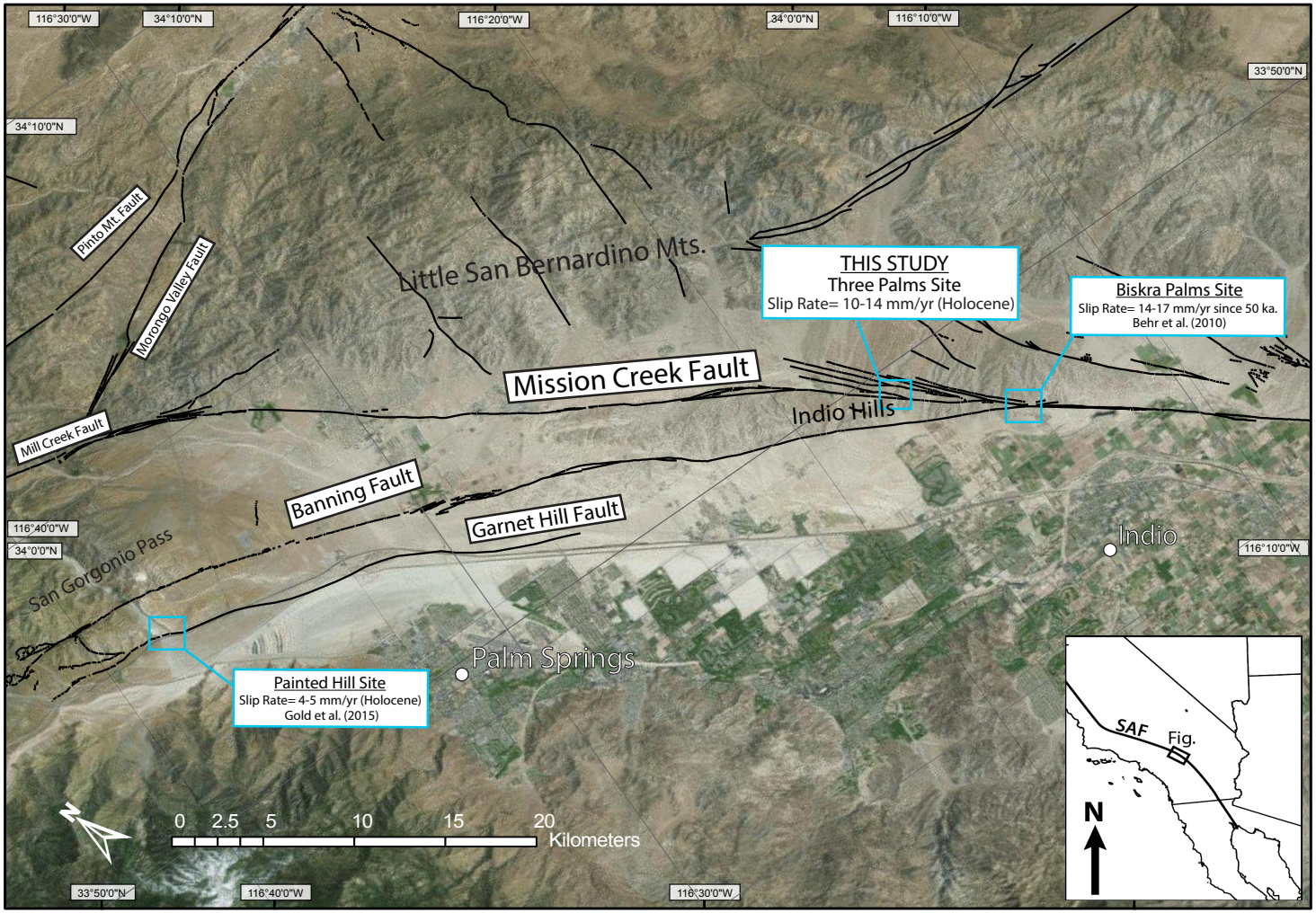

Figure 2: Map of Quaternary faults in the Coachella Valley and the eastern San Gorgonio Pass. Locations of the Pleistocene slip rate estimate from the Biskra Palms site (Behr et al. 2010) and the Holocene slip rate estimate from the Painted Hill Site (Gold et al. 2015) are shown in the map. Inset map shows location in Southern California.

2.3 Previous Geologic Slip Rate Measurements in the Northern Coachella Valley

The first geologic slip rate study in the Coachella Valley was conducted by Keller at al. (1982) and focused on a Pleistocene offset alluvial fan at Biskra Palms Oasis in the southeastern Indio Hills. These workers estimated the fan displacement and used soil age indicators (such as degree of topographic dissection, formation and preservation of desert pavement, and relative soil development) to estimate the fan age (Keller et al., 1982). The study reported an offset of 700 meters, a preferred fan age of 20-30 ka, and a minimum Pleistocene slip rate of 10-35 mm/yr, with a preferred rate of 22-35 mm/yr for the Mission Creek strand (Keller et al., 1982). This site has subsequently been revisited by numerous research teams. van der Woerd et al. (2006), for example, used field mapping complemented with topographic data, air photos, and satellite imagery to revisit the fan offset, yielding 565 $\pm$ 80 m. These workers were also the first to use cosmogenic ^{10}Be geochronology from surface cobbles to estimate the fan age, yielding 35.5 $\pm$ 2.5 ka, which, combined with the offset determination, provided a slip rate estimate of 15.9 $\pm$ 3.4 mm/yr. Behr et al. (2010) and Fletcher et al. (2010) revisited this site after the collection of the B4 LiDAR data (Bevis et al., 2005), remeasured the offset based on the LiDAR and subsurface analysis and dated the fan using U-series on pedogenic carbonate and additional cosmogenic ^{10}Be exposure dating on boulders. The age of the fan was found to be 50 $\pm$ 5 ka, with 45 ka as an absolute minimum age from pedogenic carbonate, an offset estimate of 770 +210/-90 m, and a geologic slip rate estimate of 12-22 mm/yr with a preferred rate of 14-17 mm/yr over the last 50 ka (Behr et al., 2010; Fletcher et al., 2010). The Pushawalla Palms site, 5 km west of the Three Palms site produced a Holocene geologic slip rate of 19-25 mm/yr, measured over three different time intervals (including the Holocene) over the past $\sim$100,000 years (Blisniuk et al., 2013). In 2015, a study by Gold et al., (2015) obtained a Holocene geologic slip rate estimate of 3.9 + 2.3/-1.6 mm/yr from an offset alluvial fan on the Banning fault northwest in the southeastern margin of San Gorgonio Pass using B4 LiDAR for the

displacement measurement, U-series on pedogenic carbonate dating, and ^{10}Be geochronology on surface boulders. Another study obtained a slip rate of 5.7 +2.7/-1.5 mm/yr on an offset alluvial fan located on the Banning fault in the San Gorgonio Pass that was dated using ^{14}C radiocarbon geochronology (Heermance and Yule, 2015). Results from a study on Late Quaternary alluvial fans at the eastern end of the San Bernardino Mountains in Southern California from (Owen et al., 2014) conclude that there has been no slip on the Mission Creek fault since MIS4 (71 ka). (Kendrick et al., 2015) found a slip rate of 10-12.5 mm/yr for the Pinto Mountain fault (with a lower long term slip rate) based on geologic mapping and morphometric relationships on an alluvial complex within the Mission Creek watershed. A slip rate of 0-7 mm/yr was also found on the Banning fault (Yule and Sieh, 2003). To date, there are no published Holocene geologic slip rate estimates for the Mission Creek strand, which is a missing piece of information that this thesis has addresses.

3 The Three Palms Slip Rate Site

The "Three Palms" slip rate site is located within the Indio Hills in the north-central Coachella Valley. At the southeastern corner of the Indio Hills, the relatively simple NW-striking Indio strand of the Coachella Valley segment of the southern San Andreas fault splits into the NW-striking Mission Creek fault and the W-NW striking Banning fault (Allen, 1957; Matti and Morton, 1993). The Indio Hills is a pressure ridge formed between the Mission Creek and Banning faults– the Indio Hills separate the two faults for about 23 km northwest of their convergence at Biskra Palms Oasis (Gold et al., 2015). The Indio Hills are bounded on the north by the highly distributed dextral-reverse Indio Hills fault zone and to the south by the Banning fault. The 'backbone' of the Indio Hills pressure ridge is defined by the Mission Creek fault, which forms a discrete topographic lineament. For a majority of their extent, the Indio Hills consist of uplifted and deformed Pleistocene fluvio-deltaic sedimentary rocks of the Palm Spring Formation and the reworked, only partially consolidated Quaternary fanglomerates of the fluvial Ocotillo Formation (Dibblee, 1964,

1967). Small slivers of the shallow marine Imperial Formation crop out in the northwest corner of the Indio Hills. There are several quaternary colluvium (Qc) and alluvium (Qal) deposits that are sourced from the Imperial, Palm Spring, and Ocotillo formations. Changes in surface morphology, drainage patterns and local structure from southeast to northwest in the Indio Hills indicate that there has been slip transferred from the Mission Creek strand to the Banning strand, and the Banning Strand to the Garnet Hill strand (Gold et al., 2015).

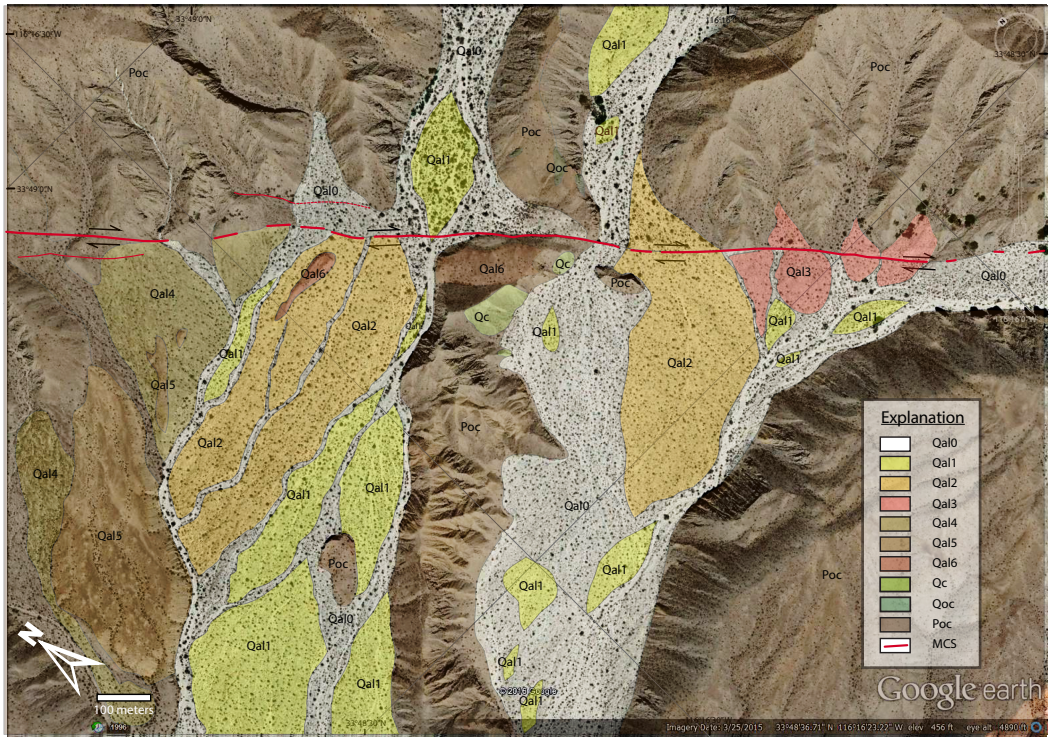

Figure 3: Geologic map of the Three Palms field area that was mapped in December 2015. Identification of alluvial units were based on degree of desert varnish, rubification of bottoms of clasts, surface roughness, and degradation of granitic boulders. MCS= Mission Creek Strand (shown in red) (See Figure 2 for location)

The Three Palms field site field area (map shown in Figure 3) consists of Ocotillo Formation (Poc) ridges that have been uplifted by the transpressive motion along the Banning fault and subsequently eroded. These ridges have been draped by colluvium (Qc) in some areas, as well as older colluvium (Qoc) that has developed a distinguishable soil and

varnish. Six quaternary fan/terrace deposits (Qal1-Qal6) were mapped in the field area– these are currently being incised by modern channels (Qal0). The Palm Spring Formation is not present in the catchment area, as the drainage only erodes through the Ocotillo Formation.

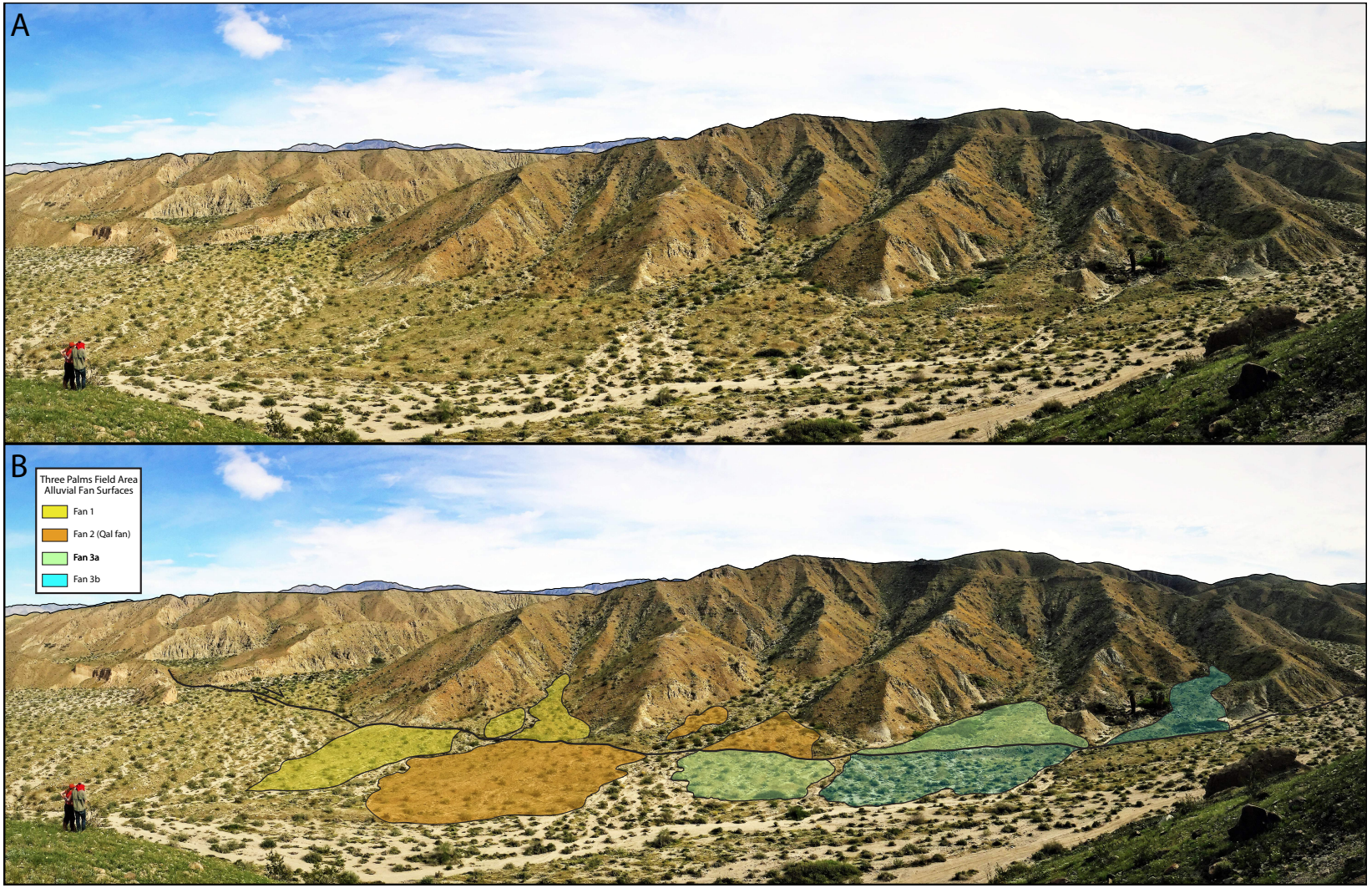

Figure 4: Figure 4A- Field panorama of the Three Palms alluvial fan. View looking N taken March 2017. Figure 4B- Interpreted geology field photo of the Three Palms alluvial fan. Qal3 fan in orange. Mission Creek fault in black.

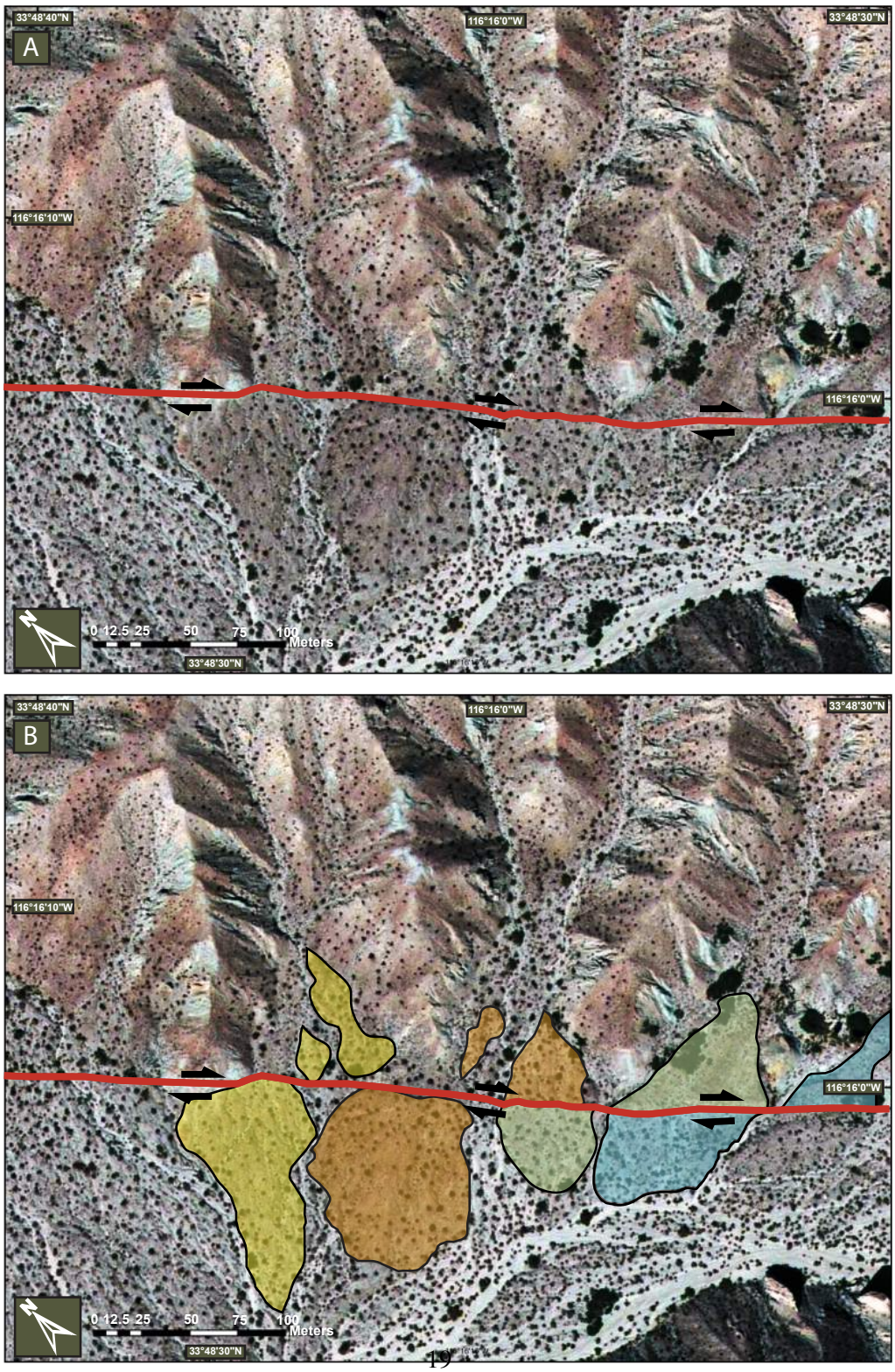

Figure 5: Figure 5A- Air photo showing the Three Palms alluvial fan and the San Andreas fault (in red) (Source of image: Google Earth) Figure 5B- Air photo with present day mapped Qal3 alluvial fan complex. The Qal3 fan is in orange.

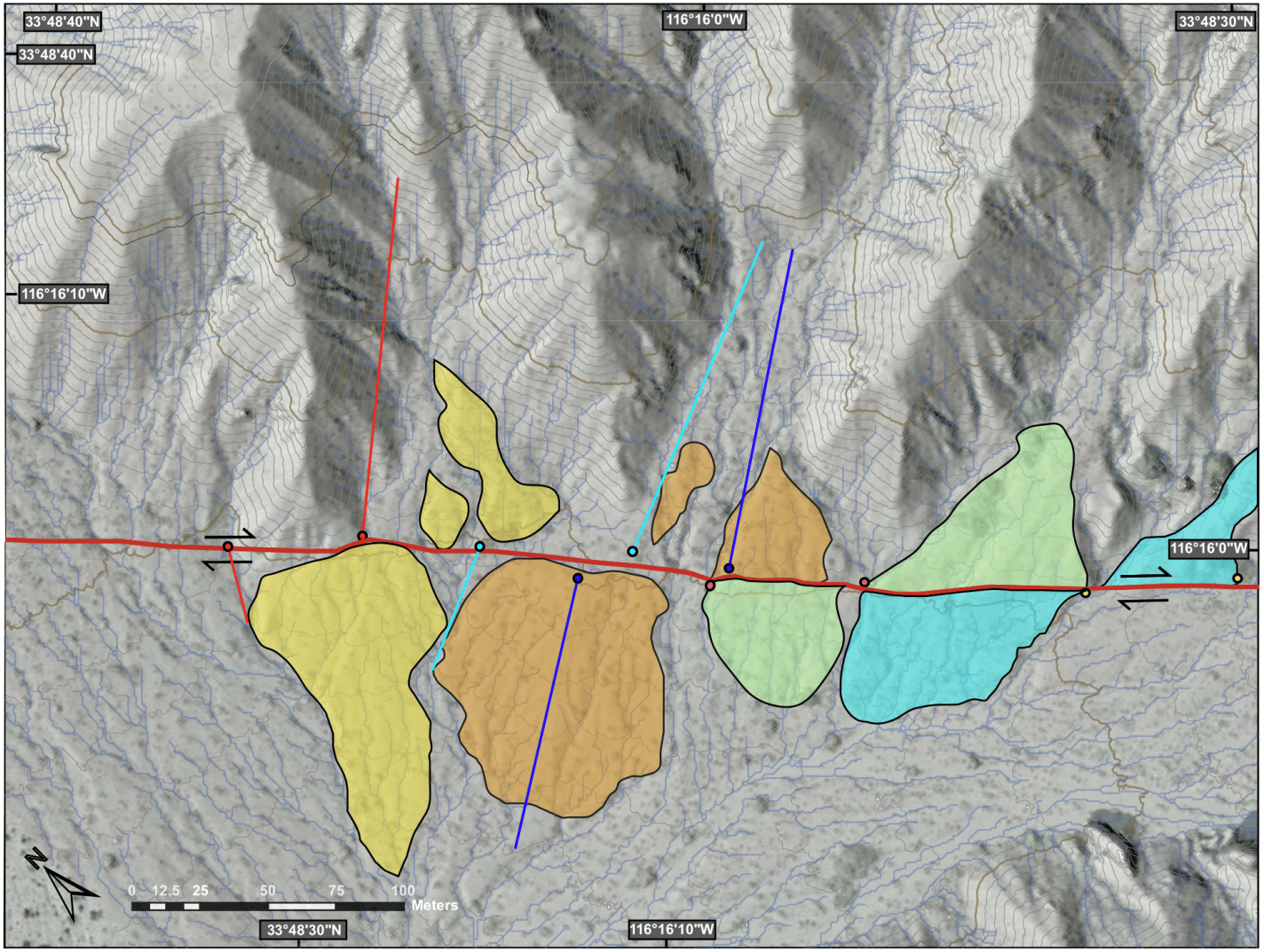

Figure 6: Present day B4 LiDAR image of the Three Palms fan complex. B4 LiDAR generated from (Bevis et al., 2005)

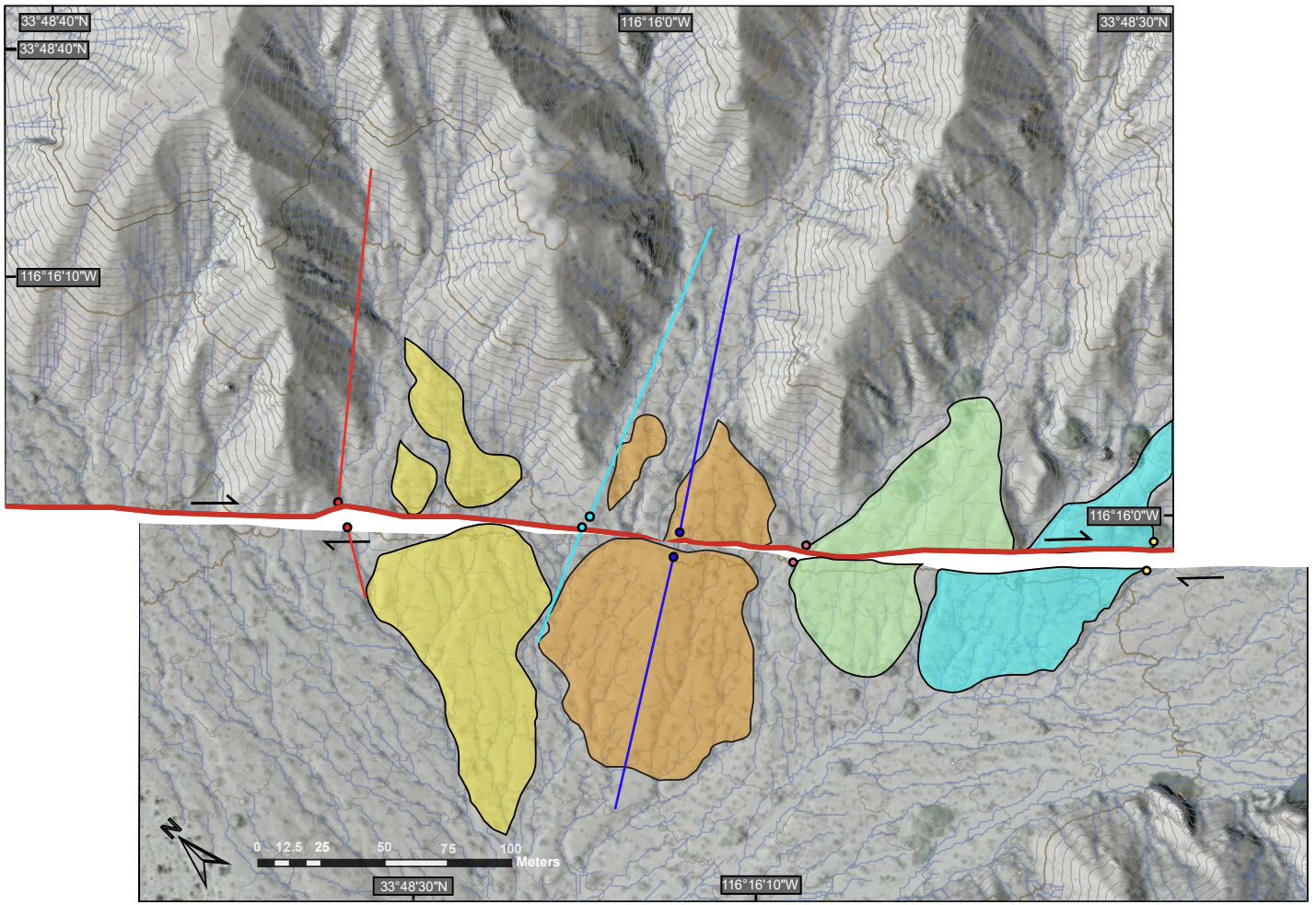

Figure 7: B4 LiDAR image of the Three Palms fan complex. Reconstructed fans show an offset of 50.0 meters

4 Offset Models

The Three Palms fan complex is composed of three small alluvial fans that have been displaced by the Mission Creek strand. The westernmost fan is sourced from a catchment length of about 215 meters; the central fan has two separate upstream channels with lengths of 315 meters and 390 meters; and the easternmost fan has a catchment length of 275 meters. The catchment of the Three Palms alluvial fan is located near the southern end of the Indio Hills, just north of the Mission Creek strand, which displaces the Three Palms alluvial fan to the south of the catchment area. Although displacement was measured using the geomorphic expression of the three fans in the field area, the geochronological data was just taken from the central fan. This study will refer to the three fans as the Three Palms fan complex within the Three Palms field area. The central fan will be referred to as the "Qal3 fan". The fan complex consists of three main components; the Ocotillo Formation, which makes up the catchment area of the fan, a Quaternary alluvium deposit, Qal which is what makes up the three fans, and younger Quaternary alluvium, Qal1 and Qal0, that incises the Qal3 fan.

The Three Palms fan complex is well visualized using available 1 meter B4 LiDAR imagery, which provides 1 meter elevation contours that are helpful in recognizing the fan morphology (Bevis et al., 2005). First, field mapping and tracing of the Three Palms fan complex was completed using the available LiDAR imagery and high resolution air photos as a guide. The Qal3 fan was then reconstructed using the following two methods: Method 1) restoring the western fan margins for all three fans to the western margin of their source catchments, and Method 2) matching the axis of the central fan to the center of its catchment.

Figure 5B shows the present day fans mapped on the aerial photo, and Figure 6 shows the same fans on a LiDAR hillshade background. First, the left piercing points of the lower Qal3 fan were reconstructed to the left extent of its modern catchment area near the upper fan (shown in red lines in Figures 6 and 7). Second, the topographic axis of the

central fan was reconstructed to the center of the central modern catchment area (shown in blue lines in Figures 6 and 7). This method is a valid method of fan reconstruction because it accounts for the erosion that the upper fan has undergone. Matching the piercing points of the lower fan to the piercing point of the upper catchment in the central fan is the proper way to reconstruct these fans since the lower fan could have been deposited from anywhere in the upper fan catchment, even if there is no remnant of that preserved fan today because of erosion. Both methods yielded the same offset determination of 50.0 meters on the Qal3 fan, as shown in Figure 7. The surrounding fans (mapped in yellow and green above) still had left and right piercing points that matched up nearly perfectly when reconstructed to 50.0 meters (shown in red, pink, and yellow points above). The fact that these two indicators match up so well on the central Qal3 fan fans is a significant and rare indicator that assures me that the offset determination of 50.0 meters is accurate. This is further validated by the near-perfect matching of the piercing points on the two surrounding fans, even though their topographic axis was not as well preserved due to erosion. In (Behr et al., 2010), the preferred offset was determined because of 2 distinct geomorphic relationships. Firstly, the preferred reconstruction was one where they curved the axial crest between the two fault strands at an angle consistent with the curvature of visible channel remnants of the reconstructed fan. Secondly, they applied negligible offset to the NE splay of the MCS in the preferred reconstruction because of 1) the intermediate and upstream sections of the reconstructed fan already had a prominent, throughgoing channel connecting them and 2) because of geochronological data that showed that the upstream T2u unit was a part of the lower reconstructed fan (T2) (Behr et al., 2010). In my study, the offset reconstruction models matched up at exactly 50.0 meters using the two methods in the above paragraph. Because there were no other measurements I could conceive as an overt quantifiable error, I apply an arbitrary 10% uncertainty bound (+/- 5.0 m) to the offset determination, but for eventual publication I intend to determine these uncertainties more quantitatively. This yielded a final offset determination of 50.0 ± 5.0 meters.

5 Geochronology

Finding surface and depositional ages for Quaternary landforms such as alluvial fans can be challenging. Before the use of quantitative methods, ages of these landforms were qualitatively determined by observing features such as soil profile development and degree of topographic dissection (Keller et al., 1982; Mayer et al., 1988). With the development of quantitative Quaternary geochronology, there are several new methods to constrain the age of landforms. Two geochronometers were used to date the Qal3 fan; U-series on pedogenic carbonate rinds and cosmogenic ^{10}Be surface exposure geochronology on surface boulders and cobbles.. The U-series sample collection and preparation was conducted by UT undergraduate student Rosemarie Fryer as part of her senior thesis for the Undergraduate Honors Research Program and the measurements were conducted at BGC by Dr. Warren Sharp– below I summarize her methods and results. My own contribution to the geochronology focused on sampling, sample preparation and processing for cosmogenic dating. Final sample processing (column chemistry) was completed by UT Ph.D. Candidate Peter Gold and ^{10}Be measurements were conducted at Lawrence Livermore National Laboratory.

5.1 U-series Dating on Pedogenic Carbonate

Theory

Pedogenic carbonate consists of $CaCO_3$ and minor amounts of $MgCO_3$, and is commonly found in calcic soils (Machette, 1985). Pedogenic carbonate coatings accumulate in layers on the undersides of coarse grained clasts in calcic soils subject to arid and semiarid temperatures (Gile et al., 1965; Machette, 1985; Fletcher et al., 2010). Since arid regions compose over a third of the global terrestrial environment (Capo and Chadwick, 1999) these types of soils and carbonate formation are common, and are found in many areas of the western United States (Machette, 1985; Fletcher et al., 2010). Carbonate precipitation

typically occurs at depths of 30-200 cm (Fletcher et al., 2010). This depth is controlled by factors such as climate; wetter climates generally signify increased carbonate formation depth. However; a bimodal distribution has been observed for soils on an alluvial fan in the Providence Mountains piedmont in the Mojave National Preserve. In this study, McDonald and others (1996) noted that the upper 75 cm of soils in southern California correspond to Holocene carbonate formation while everything below this threshold corresponds to Pleistocene carbonate formation. This bimodal distribution can be strongly linked to substantial changes in precipitation (McDonald et al., 1996).

Sample name	Sample wt (mg)	U (ppb)	^{232}Th (ppb)	^{230}Th/^{232}Th	^{232}Th/^{238}U	±%	^{230}Th/^{238}U	±%
TP-4	1.6	5146	650.8	0.722	0.0409	0.26	0.0214	10.4
TP-5	5.1	3379	1704	0.641	0.1459	0.39	0.09	2.6
TP-6	3.3	4323	278	1.798	0.0209	0.52	0.0327	4.8
TP-9A	1.5	7744	3450	0.397	0.1442	0.48	0.0512	4.8
TP-9B	1.7	7632	1434	1.308	0.0612	0.45	0.0748	2.6
TP-10	2.1	8437	3430	1.289	0.1317	0.5	0.1659	1.1
TP-11A	2.9	5023	6444	0.185	0.415	0.38	0.0723	2.5
TP-11B	2	6048	4373	0.28	0.2348	0.38	0.0602	3.1
TP-12A	3.1	4384	805.9	1.389	0.0593	0.35	0.0773	2.6
TP-12B	2.6	4586	466	1.837	0.0328	0.49	0.548	4.5
TP-12C	2.2	4215	542.8	1.678	0.0418	0.48	0.063	3.8

Table 1: Table 1 shows the U-series analytical data and ages for pedogenic carbonate from offset fan at Three Palms Site. (Fryer, 2016)

Sample name	$^{234}U/^{238}U$	±%	Uncorrected age (ka)	Error (ka)	Corrected Age (ka)	Error (ka)	Initial Age $^{234}U/^{238}U$	Error
TP-4	1	0.76	2.38	0.25	*	*	*	*
TP-5	1.012	0.46	10.15	0.29	*	*	*	*
TP-6	1.01	0.48	3.59	0.18	1.95	0.86	1.0106	0.0052
TP-9A	1.024	0.78	5.6	0.29	*	*	*	*
TP-9B	1.027	0.47	8.24	0.23	3.1	2.7	1.0288	0.0072
TP-10	1.005	0.51	19.67	0.28	7.5	6.6	1.0057	0.0135
TP-11A	1.013	0.31	8.07	0.22	*	*	*	*
TP-11B	1.015	0.6	6.67	0.22	*	*	*	*
TP-12A	1.026	0.47	8.54	0.24	3.5	2.6	1.0273	0.0071
TP-12B	1.021	0.48	6.01	0.28	3.3	1.4	1.0217	0.0057
TP-12C	1.019	0.48	6.96	0.28	3.6	1.8	1.0201	0.006

Table 2: Table 2 shows the U-series analytical data and ages for pedogenic carbonate from offset fan at Three Palms Site. * = age was not produced from sample. (Fryer, 2016)

Accumulation of pedogenic carbonate in coarse-grained deposits occurs in a well-documented progression, with the youngest rinds forming at the bottoms of the clasts (Machette, 1985; Mayer et al., 1988; Fletcher et al., 2010). The lack of leaching and extensive rainfall leads to the lateral formation of pedogenic calcium carbonate, which occurs in cemented layers known as calcrete (Capo and Chadwick, 1999). When these soils form, water percolating into the soil horizons from the surface dissolves calcium (Ca^{+2}) ions from rainwater, dust, and other sources and leaches them along with trace amounts of uranium (U) into lower soil horizons (Gile et al., 1965; Machette, 1985; Capo and Chadwick, 1999). Trace amounts of U come from silicate and oxide dust particles that have settled at the surface and in the soil as detrital matter (Schwarcz, 1989). Initially, this U occurs in an insoluble UIV (quadrivalent ion), but is oxidized into the UVI (hexavalent) ion at the surface. This ion forms water soluble complexes with bicarbonate, which is dissolved in the soil from carbon dioxide derived from plant respiration and the atmosphere (Schwarcz, 1989). The trace U-bicarbonate complex combines with Ca^{+2} ions and forms calcium carbonate ($CaCO_3$) rinds on the bottoms of clasts when the soil desiccates. Since these pendant water films with $CaCO_3$ deposit multiple times on the same surface over time, the pedogenic carbonate will form in layers known as rinds. The U is precipitated in trace amounts in the $CaCO_3$, where it allows previously formed ^{230}Th daughter isotopes to separate, providing a new crop of daughter isotopes in the $CaCO_3$ (Schwarcz, 1989). This process, along with U's initial insolubility in groundwater, limits the amount of inherited ^{230}Th in the pedogenic carbonate, which makes it possible to accurately determine the time elapsed since the precipitation of the carbonate.

The uranium disequilibrium method, or U-series dating, can be used to determine the age of carbonate precipitation by $^{230}Th/^{234}U$ and $^{234}U/^{238}U$ activity ratios using the following equation (Schwarcz and Latham, 1989):

$$\frac{^{230}\mathrm{Th}}{^{234}\mathrm{U}} = \frac{^{238}\mathrm{U}}{^{234}\mathrm{U}}[1-\exp(\lambda t_0)] + \left[\frac{\lambda t_0}{\lambda_0 - \lambda_4}\right]\left(1 - \frac{^{238}\mathrm{U}}{^{234}\mathrm{U}}\right)[1-\exp(\lambda_0 - \lambda_4)t] \qquad (1)$$

where t is the age and λ_0 and λ_4 are decay constants for ^{230}Th and ^{234}U, respectively. However, there are two basic assumptions that should be satisfied when using this method: the first assumption is that the sample dated has been in a closed system, and the second is that the daughter/parent ratios (i.e., the ^{230}Th/^{234}U and ^{234}U/^{238}U ratios) were zero or another determinable ratio during the time of formation (Schwarcz, 1989). Using this method, the oldest rinds of the carbonate coating should best approximate the age of fan deposition. More recent studies have analyzed these samples by utilizing thermal ionization mass spectrometry (TIMS) (Fletcher et al., 2010; Fryer, 2016).

Sampling and Sample Processing

In this study, 45 clasts were collected on the Qal3 fan and processed at the Berkeley Geochronology Laboratory. Since the $CaCO_3$ coatings in this field area were particularly thin, the entire coatings were included in the analysis and averaged using the following procedures, as documented in (Fryer, 2016). The clasts were first cleaned with tap water and a toothbrush to remove dust particles and detrital grains from coatings. The clasts were then sorted based on visual abundance and purity of the carbonate present. After this qualitative filter, only 15 samples were further processed. After removing the carbonate coats with a steel blade under a microscope, they were cleaned of excess detritus with tweezers and ultrasonic cleaning in alcohol. The eleven samples were weighed and placed in glass tubes. They were then dissolved with concentrated HNO_3 and HF before a mixed spike of ^{233}U, ^{236}U, and ^{229}Th was added to each sample. Uranium and thorium were separated using anion exchange columns, then analyzed using conventional TIMS techniques in single ion counting mode (Sharp et al., 2003). Ages were calculated using the half-lives of (Jaffey et al., 1971) for ^{238}U, (Senftle et al., 1956) for ^{232}Th, and (Cheng et al., 2013) for ^{230}Th and

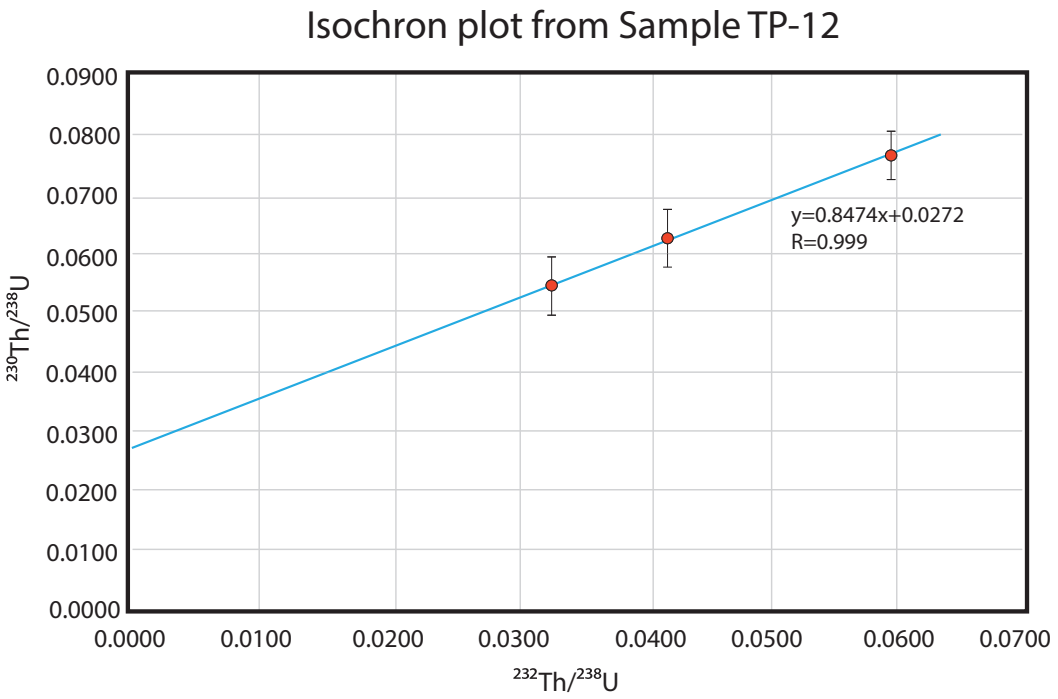

Figure 8: Isochron plot from sample TP-12 comparing ^{230}Th/^{238}U to ^{232}Th/^{238}U, this ratio is linear across the three samples indicating the growth of the carbonate rind was a closed system (Fryer, 2016).

^{234}U. Correction for U and Th from detritus was made from assuming detritus with activity ratios of (^{232}Th/^{238}U) = 1.21 $\pm$0.50, (^{230}Th/^{238}U) = 1.0 $\pm$ 0.1 and (^{234}U/^{238}U) = 1.0 $\pm$ 0.1, which correspond to average silicate crust in secular equilibrium. Initial (^{234}U/ ^{238}U) is calculated from the measured ratio and the corrected ^{230}Th age. Uncertainties of corrected ages include analytical errors and the detritus correction uncertainties. Table in the appendix contains values used for the initial ^{230}Th/^{232}Th ratio for calculating ages.

Results

The dates that were acquired from the study were 3.3 $\pm$ 0.6 ka (95% CI) model independent isochron age for the youngest sample (Figure 8). Using a standard correction for the five oldest samples, the mean weighted age of these samples was 3.49 $\pm$ 0.92 ka

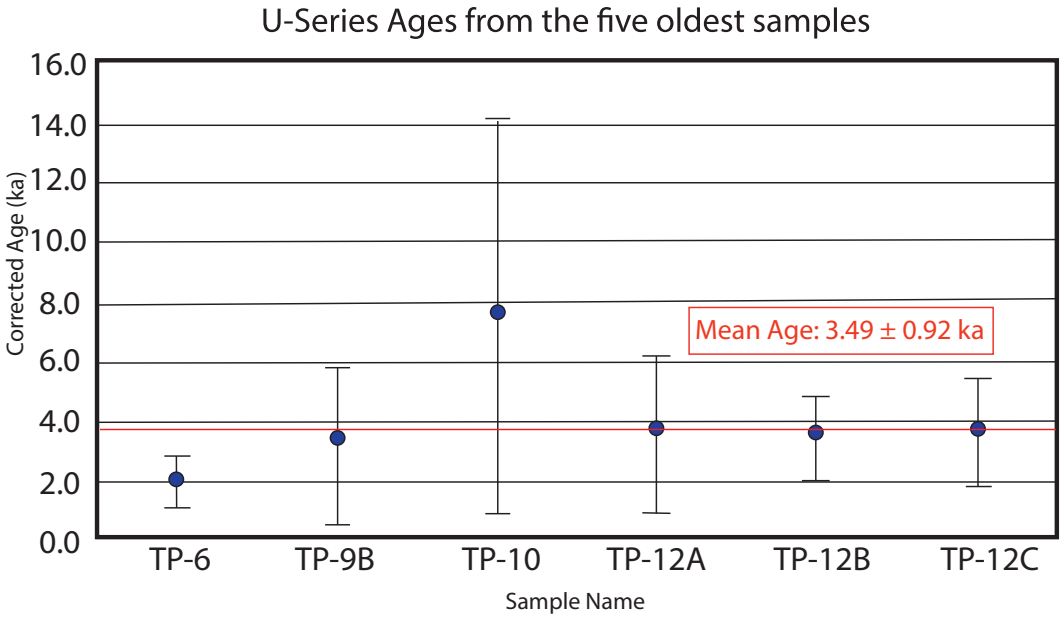

Figure 9: Uranium series ages of oldest pedogenic carbonate samples. Error bars indicate 2σ uncertainty. The red line shows the weighted average of 3.49 ± 0.92ka (95% CI) from the five oldest samples. (Fryer, 2016)

(95% CI) (Figure 9). This provides a reliable bound for the minimum depositional age for the host fan, which was then compared to the age acquired from the surface exposure dating.

5.2 Cosmogenic ^{10}Be Surface Exposure Dating

Theory

In the last twenty years, the increased development of cosmogenic ^{10}Be surface exposure dating has allowed it to emerge as one of few reliable methods for dating Quaternary-aged surfaces. Although successfully used in glacial terranes, the application of this technique in arid alluvial surfaces has also gained legitimacy in finding their depositional age and determining erosion rates in fluvial environments. However, there are many caveats to this method of dating, both inherent to assumptions about nuclide production rates to

systematic biases introduced with different sampling methods and clast sizes.

The production of ^{10}Be comes from high energy galactic cosmic radiation (GCR) that is emitted from supernovas and other energy releasing events in the universe. This GCR is composed of mostly protons and neutrons, and it eventually combines with lower energy particles produced from the sun and penetrates the earth's atmosphere, filtering through the earth's magnetic field, and showering on the earth's surface as secondary GCR (Dunai, 2010). Most cosmogenic nuclides form when neutrons in the secondary GCR impact rocks and minerals through a spallation reaction, which is where a high-energy neutron collides with a nucleus on the target material. This collision causes the nucleus of the target atom to break ("spall") into smaller nuclei by clustering together after the shattering of the original nucleus (Gosse and Phillips, 2001). In the case of ^{10}Be, quartz (SiO_2) particles are shattered by this secondary GCR and spall into ^{10}Be (from ^{16}O) and ^{26}Al (from ^{28}Si). Because these rare nuclides are mostly produced from these cosmogenic spallation reactions on earth, measuring their concentration can be used as a proxy for the exposure age of the quartz to the surface.

Although cosmogenic ^{10}Be can be used in various applications, e.g., (Lal, 1991; Morris, 1991; Gosse and Phillips, 2001), in recent years the measurement of these nuclides has been used as a direct dating method for time that a geomorphic feature or landform has been exposed to the surface. Attaining reliable dates from the concentrations that are measured can be completed with a variety of methods. The simplest and most commonly used method to measure the age of a surface is to directly measure the ^{10}Be concentration of boulders, cobbles, pebbles, and/or sand on that surface. The application of this method is somewhat complex, as it is important to consider numerous attributes of the sample taken, such as the shielding it undergoes, its quartz content, and its size.

One of the most significant issues when dating arid alluvial fans using cosmogenic ^{10}Be is the issue of inheritance. "Inheritance" refers to the concentration of pre-depositional (or "inherited") ^{10}Be that the sample might have acquired prior to its incorporation into the

deposit of interest (e.g. on hillslopes of the host catchment, or eroded from an older deposit upstream) (Lal, 1991). To fully understand the effect of inheritance on samples, one must understand the depositional history of the samples. Since it is nearly impossible to monitor the exact exposure history of a boulder on a fan surface from its original exposure to its final deposition location, studies must employ a sampling strategy to account for this inherited component of ^{10}Be. There are three common ways to attempt to address inheritance 1) sample a depth profile, 2) take samples from the modern wash, or 3) assume zero inheritance on the youngest date.

Depth profiles involve sampling pebbles or cobbles at intervals down to two meters beneath the deposit of interest. The predicted curve of the profile should show an exponential decrease in ^{10}Be concentration with depth, until it reaches an asymptote where the production rate is zero. This asymptote can be interpreted as the inherited signal for the deposit, as it should show the residual ^{10}Be that exists below the maximum attenuation depth of 2 m (Anderson et al., 1996; Repka et al., 1997; Gosse and Phillips, 2001). Many processes can disrupt the predicted curve, however, including surface erosion, bioturbation, multiple deposits within the profile, eolian input of new sediment, and/or different inheritance histories for different clast sizes (Anderson et al., 1996; Repka et al., 1997; Phillips et al., 1998; Gosse and Phillips, 2001; Densmore et al., 2007; Hidy et al., 2010). Anderson et al., 1996 was the first study that proposed to incorporate depth profiles to account for inheritance, while Repka et al., 1997 used amalgamated samples of cobbles of river terraces to account for the stochastic nature of burial depth and hence in nuclide production in these clasts. Although it is difficult to predict the variability of these sample ages, these two classic studies led the way for the modern interpretations of ^{10}Be depth profiles. For example, Hidy et al., 2010, used a Monte Carlo approach to accurately simulate and analyze the stochastic nature of ^{10}Be ages in depth profiles.

In areas whose cosmogenic nuclide concentrations have not come to equilibrium, it has been determined that their depth profiles will often converge to a unique mixture of

inheritance, erosion rate, and exposure ages when accounting for both muogenic and nucleogenic pathways (Braucher et al., 2009). A very thorough soil description is also important when constructing a depth profile because it can shed light on the area's depositional history, as well as explain any anomalies that the depth profile might yield (Gosse et al., 2003). Studies have also amalgamated cobbles in depth profiles to accurately determine the effect of inheritance on river terraces. Numerical modeling using plausible exhumation and transport scenarios suggests that 30 cobbles are sufficient to constrain the mean to within 5 percent (Repka et al., 1997) Although depth profiles of amalgamated samples allow us to constrain the effect of mean inheritance, sediment mixing, and estimate the age of the surface of interest (Repka et al., 1997), it is evident that their results are dependent on and can be disrupted many factors on the depositional environment.

Another method that has been used to estimate inheritance involves collecting and measuring samples from the modern wash. (Gosse et al., 2003; van der Woerd et al., 2006; Frankel et al., 2007a; Blisniuk et al., 2010; Armstrong et al., 2010; Behr et al., 2010; Owen et al., 2011; Blisniuk et al., 2012). Assuming these samples were very recently deposited, if there is no inheritance, they should theoretically have a ^{10}Be depositional age of zero; otherwise, the amount of ^{10}Be may approximate the average inheritance for the catchment area. One could then subtract the date produced by this method by the age acquired from dating the fan to find the true depositional age of the fan. If the modern wash age is older than the samples, this means that the amount of inheritance cannot be quantified. However, this also signifies that the field area has a high inherited ^{10}Be component (Frankel et al., 2007a).

The third method is to take the minimum ^{10}Be date as the maximum depositional age for the fan (assuming zero inheritance). A review of published quaternary geochronologic data by (Gold and Behr, 2016) concluded that although estimating inheritance by using depth profiles or modern wash sample measurements can be useful, only in rare cases can an inheritance date be quantified from these methods. Therefore, taking the minimum

^{10}Be date as a maximum fan depositional age is the most reliable and conservative method in constraining the amount of inheritance in an arid region alluvial fan. Naturally, it is most effective when many ($<$15) cosmogenic samples are taken.

Sampling and Sample Processing

A clast size range (large cobbles to small boulders) was targeted for sampling from the Qal3 fan to avoid any dating uncertainties associated with clast-size-dependent exposure or inheritance histories. More specifically, I attempted to avoid date variability due to clast-size dependence of inheritance. I also collected one amalgamated cobble sample from the lower fan to compare this with that of surface boulders, and an amalgamated sand and boulder sample from the modern wash to attempt to account for an average inherited component for the catchment area of the Qal3 fan.

Since the field area had very little vegetation or extremely steep topographic relief near the samples, a long effect of shielding was not an issue. Since possible snow cover effects were null, a seasonal shielding factor to account for production rate variation was not issued. The samples taken were boulders and cobbles on the Qal3 fan that were sourced from the loosely consolidated fanglomerate Ocotillo formation. The clasts within the Ocotillo formation are sourced from Precambrian metasedimentary rocks and Jurassic/Cretaceous granitoid rocks. Although the schistose samples that were collected in the field had higher amounts of mica, they still had sufficient amounts of quartz for effective ^{10}Be measurement.

The surface boulder samples were collected using the specifications outlined by Gosse and Phillips (2001). Some of the specifications included collecting larger samples that are high above the fan because of the effects of erosion on ^{10}Be concentration described above, collecting flat and horizontal samples because of the effects of self-shielding and changes in cosmic ray flux that have to be taken into consideration, and collecting samples that are not shielded topographically or by vegetation (the latter of which was not an issue

because of the flat topography and the barren landscape of the field area). After identifying the surface boulders to be collected, the upper five centimeters of the boulder were chipped off using a mini sledge hammer and chisel. This is because there are no attenuation effects in the upper five centimeters of a rock surface (Gosse and Phillips, 2001). A sand sample from the modern wash was collected, as well as an amalgamated cobble sample from the lower fan. There were a total of 14 samples collected.

The 14 samples were then transported to the University of Texas at Austin where they were crushed, disc milled, and sieved to 250-500 μm using standard procedures. They were then taken to the Arizona State University Cosmogenic Nuclide Laboratory in the spring and summer of 2016 for further processing in preparation for ^{10}Be analysis at the Center for Accelerated Mass Spectrometry at Lawrence Livermore National Laboratories. The processing procedures are delineated as an appendix, but a summary of these procedures is provided below.

Samples were placed in Nalgene bottles and underwent four HF leaches for nine hours per leach at different concentrations to isolate quartz, the most chemically resistant mineral in the samples and the one necessary for ^{10}Be analysis. Between the first and second leaching, froth flotation techniques were also effectively used to separate feldspar from quartz. After the four cycles of leaches and cycle of froth flotation, it was necessary to test if the remaining samples were purely quartz. To make sure of this, I needed to test the Al concentration in the samples. Aliquots were prepared using a procedure (detailed in the appendix) that leached the samples using separate concentrations of $HClO_4$, HF, and HCl. The samples passed assay, and anion exchange column chemistry procedures were performed to separate pure quartz from the sample. The quartz was then sent for ^{10}Be analysis at the Center for Accelerated Mass Spectrometry at Lawrence Livermore National Laboratories. Results were received in September 2016.

Inheritance for the Three Palms fan surface samples was considered for by using the three techniques described in the Theory section. The depth profile method was attempted

after digging the trench on the lower Qal3 fan. The debris flow deposit that defines the Qal3 fan was only a meter thick. Multiple debris flows within the upper two meters (which is the depth required for a viable depth profile) of the deposit would produce an irregular depth profile that would have given zero quantifiable information about the surface age or the inherited ^{10}Be component of the deposit. Therefore, a depth profile was not constructed for this project.

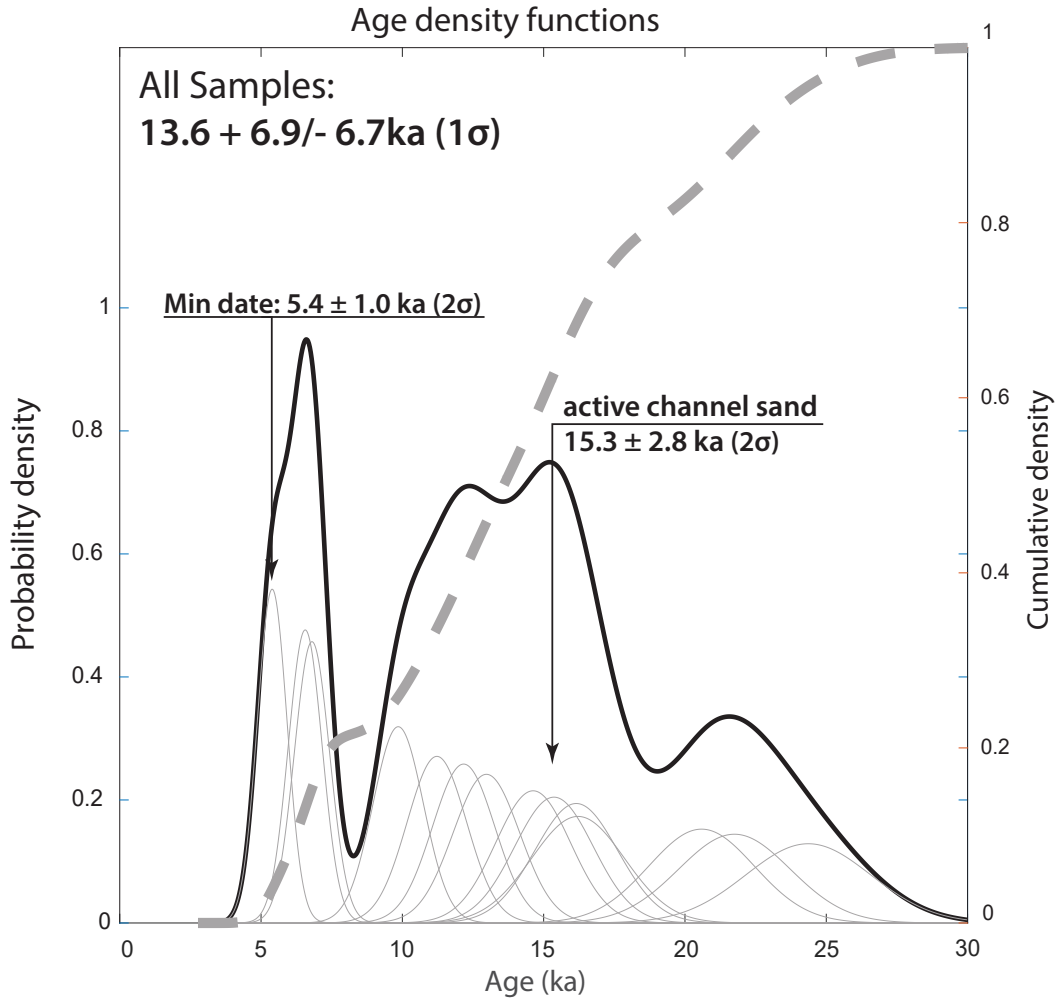

Figure 10: Probability density function (PDF) of all 14 samples collected on the Qal3 fan. Gray curves are gaussian uncertainty PDF curves for individual samples. Gray dotted line is the cumulative density function for all samples. Figure generated from MATLAB code in (Zechar and Frankel, 2009).

Sample	Clast Type	Height (cm)	Latitude (°N)	Longitude (°W)	Elevation (m)	Spall.	Age (yrs)	Ext 2σ Error$\pm$(yrs)	Int 2σ Error$\pm$(yrs)
MTP 1	Boulder	19.8	33.80833	-116.268611	149.962	3.91	6802	623	223
MTP 2	Boulder	11.8	33.80829	-116.268621	149.950	3.91	20587	1868	606
MTP 3	Boulder	17.3	33.80889	-116.269167	149.657	3.91	24364	2212	717
MTP 4	Boulder	5.2	33.80887	-116.269166	149.642	3.91	9854	893	295
MTP 5	Amal. Cobbles	2	33.80833	-116.268621	149.720	3.91	11222	1052	429
MTP 6	Boulder	11.7	33.80833	-116.268611	150.000	3.91	12169	1103	361
MTP 7	Boulder	17.5	33.80833	-116.268611	150.150	3.91	5394	525	250
MTP 8	Boulder	6.4	33.80833	-116.268889	148.438	3.90	21751	1975	644
MTP 9	Boulder	15.2	33.80833	-116.268889	148.488	3.90	16154	1467	484
MTP 10	Boulder	8.9	33.80833	-116.268689	149.030	3.90	16216	1645	879
MTP 12	Boulder	11.4	33.80806	-116.267888	153.619	3.92	6563	598	208
MTP 13	Amal. Sand	0	33.80852	-116.267488	154.020	3.92	15365	1393	455
MTP 14	Amal Boulder	4	33.80852	-116.267488	154.100	3.92	12975	1179	394
MTP 15	Boulder	21.5	33.80806	-116.268056	149.850	3.91	14627	1326	433

Table 3: Table of 14 samples collected for ^{10}Be analysis. Field and production rate data. Density for all samples was 2.7 g/cm^3 Shielding factor for all samples was 1. Spall= Spallation production rate, measured in atoms /g^{-1}a^{-1}. Muon production rate for all samples was 0.079 atoms /g^{-1}a^{-1}. Height measurement signifies the height of the sample above Qal3 surface. Thickness for all samples was 4 cm. Data processed using Cosmic-Ray Produced Nuclide Systematics on Earth (CRONUS-Earth) project software and graphed using the MATLAB code from (Zechar and Frankel, 2009).

Sample ID	^{10}Be/^{9}Be	^{10}Be/^{9}Be 1σ error	Blank	Sample Wt.(g)	Carrier Wt. (g)	[^{10}Be] atoms/g qtz	Error 2σ $\pm$atoms/g qtz
MTP 1	6.595E-14	1.463E-15	4	50.5259	0.3029	27073.184	1769.228
MTP 2	2.005E-13	3.741E-15	4	50.0884	0.2948	81663.289	4784.308
MTP 3	2.621E-13	4.902E-15	4	50.1418	0.2665	96529.377	5648.829
MTP 4	9.619E-14	1.816E-15	4	50.7557	0.3005	39183.549	2340.445
MTP 5	1.127E-13	3.408E-15	4	50.2282	0.2885	44610.382	3399.601
MTP 6	1.240E-13	2.321E-15	4	51.3982	0.2908	48373.517	2858.832
MTP 7	5.463E-14	2.116E-15	4	50.3656	0.2902	21479.866	1990.321
MTP 8	2.149E-13	4.070E-15	4	50.8911	0.2947	86146.558	5074.901
MTP 9	1.506E-13	2.908E-15	4	48.2882	0.2973	64069.352	3821.256
MTP 10	6.776E-14	3.213E-15	2	21.7217	0.3053	64346.333	6950.437
MTP 12	6.467E-14	1.335E-15	5	50.3679	0.3037	26203.855	1657.759
MTP 13	1.465E-13	2.744E-15	5	50.1127	0.3058	61233.733	3612.538
MTP 14	1.260E-13	2.486E-15	5	50.8311	0.3054	51745.228	3129.561
MTP 15	1.396E-13	2.616E-15	5	50.0737	0.3043	58100.170	3430.517

Table 4: Table of 14 samples collected for ^{10}Be analysis. Lab analysis results. Blank = Blank ^{10}Be/^{9}Be concentration and 1σ error. 2= 1.964E15$\pm$3.756E-16; 4= 1.035E-15$\pm$5.02E-16; 5= 2.194E-15$\pm$4.417E-16. Data processed using Cosmic-Ray Produced Nuclide Systematics on Earth (CRONUS-Earth) project software and graphed using the MATLAB code from (Zechar and Frankel, 2009)

.

Results

The 14 samples dated yielded a mean age of 13.9 ka with a median age of 13.6 +6.9/-6.7 ka (1σ error) (see Tables 3 and 4) This average was determined using a Gaussian uncertainty model for the individual sample probability distribution functions (shown in gray dotted lines in Figure 10) using the MATLAB code of (Zechar and Frankel, 2009). A probability distribution function is a graph of a continuous random variable whose value at any sample point can be interpreted as providing the relative likelihood that the point will equal that value. This graph also contains a cumulative density function, which shows the probability that a random variable evaluated at a point, will take a value less than or equal to that point. The modern wash sample had an older date (15.3 ± 1.4 ka (1σ error)) than the average. This observation, combined with the significant amount of scatter in the Qal3 cosmogenic dataset only to determine a maximum depositional age for the fan, using the youngest sample date of 5.4 ± 1.0 (2σ error)

5.3 Geochronometer Consistency and Interpreted Depositional Age

Interpreting the depositional age of an arid alluvial fan is complicated since the geochronometers that are used have differing degrees of uncertainty. Since the geochronometers produce minimum and maximum age bounds to bracket the depositional age of the fan surface, we need to know that both geochronometers are consistent with one another. For example, they might be inconsistent because of the differing degrees of uncertainty and reporting styles that ^{10}Be and U-series data work with, as well as the differing geologic variables that yielded the results for both datasets. The consistency of both methods must be validated to correctly interpret the surface depositional age of the Three Palms fan. The datasets reveal that both geochronometers used in this study were consistent and produced a well constrained interpreted depositional age range.

The average U-series date serves as a consistent minimum depositional age constraint for two primary reasons: First, a minimum depositional age constraint of 3.5 ka cou-

pled with an assumedly valid ^{10}Be maximum depositional age constraint of 5.2 ka would yield a maximum carbonate lag time of 1.9 ka. Although there has not been a published estimate for the carbonate lag time southern California (Fletcher et al., 2010), previous estimates of carbonate lag time in fluvial gravels include 5 $\pm$ 5 ka in the Rocky Mountains (Sharp et al., 2003) and 2 $\pm$ 1.5 ka on the Tibetan Plateau (Blisniuk and Sharp, 2003). This indicates that carbonate lag time in arid to semiarid environments with Holocene timescales are generally short, leaving the max carbonate lag time of 1.7 ka yielded in this study to be entirely plausible, and leaving the minimum depositional age only a couple of thousand years from the true depositional age of the fan surface. Second, although the dates on clast-coatings yield an average age that may have formed over several ka (Fletcher et al., 2010; Blisniuk et al., 2012), the rinds that were analyzed on the pedogenic carbonate samples collected in this study were very thin, which indicates (as well as their U-series age) that they are very young. These thin rinds likely formed during a single wet cycle, further validating that the date produced from the U-series geochronology is a well constrained minimum depositional age.

The ^{10}Be age is likely a valid maximum depositional age constraint because of two other primary reasons: First, since erosion/aggradation rates in this arid environment are significantly low (-0.7-0 mm/ka according to (Frankel et al., 2007a), evidence for significant surface lowering (e.g. of sediment around the sampled clasts) within a Holocene time scale is not present. Although none of the boulders sampled were over 50 cm above the surrounding sediment, there is no evidence for scaling of clast ages with height as would be expected if the fan had experienced significant erosion to expose these clasts with time. Second, since erosion rates are so low, the boulder erosion rates required to remove the ^{10}Be concentration attributed to the mean of all the samples dates (13.9 ka) to the minimum date (5.4 ka) would be impossible. Because of this, there is significant evidence that shows that the dataset produced from this young fan is inheritance-dominated and not governed by a balanced, erosion dominated system. Because of the evidence supporting the accurate

interpretation of the average U-series and minimum dates as the respective minimum and maximum fan depositional ages, the two geochronometers in this case agree with each other and are highly complementary. They also suggest a carbonate lag time of less than 2 ka.

6 Holocene Geologic Slip Rate

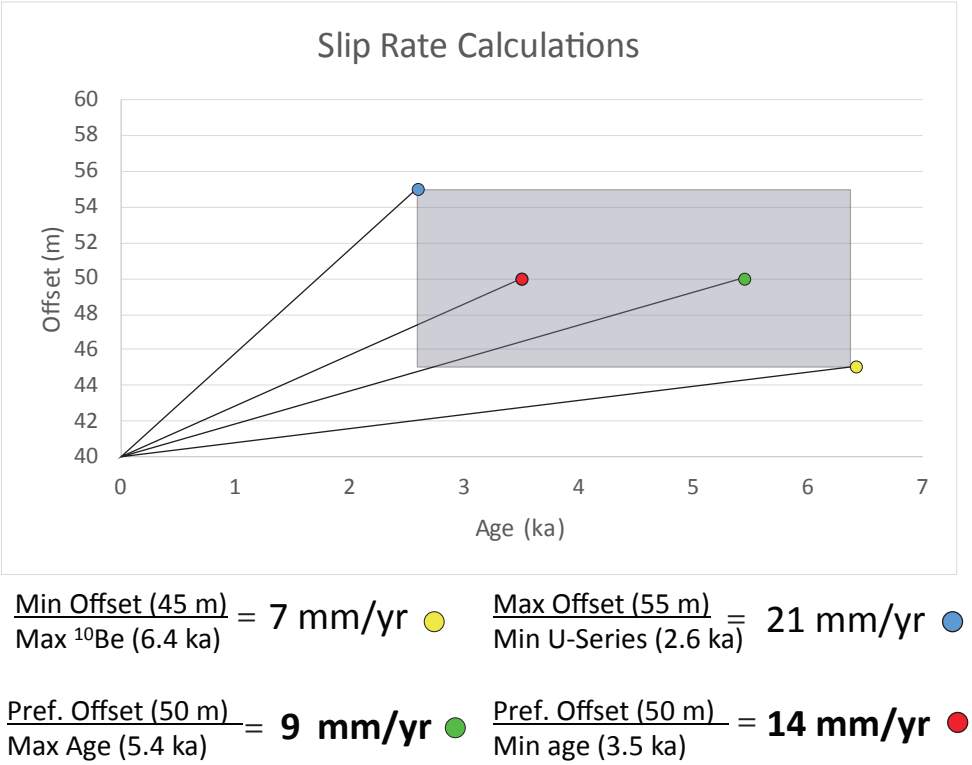

Figure 11: Graph showing the minimum and maximum slip rate (Offset/ Fan Age) calculations in yellow and blue, respectively, with a gray box that represents the entire range of slip rates that are possible given the results. The preferred minimum and maximum rates are shown in red and green, respectively.

After determining the offset amount, minimum depositional age from the U-series, and maximum depositional age from the cosmogenic ^{10}Be dating, I calculated the slip rate estimate. To calculate the minimum possible slip rate, the minimum offset uncertainty

bound (45.0 meters) was divided by the maximum ^{10}Be 2σ uncertainty bound date (6.4 ka) to produce a slip rate of 7 mm/yr. The maximum possible slip rate was calculated by dividing the maximum offset uncertainty bound (55.0 meters) from the minimum U-series 2σ uncertainty bound date (2.6 ka) to produce a slip rate of 21 mm/yr. This provided an estimated range of 7-21 mm/yr. To calculate the preferred slip rate estimate, the preferred offset (50.0 meters) was divided by the maximum depositional age (the min ^{10}Be date of 5.4 ka) and the minimum depositional age (the mean U-series date of 3.5 ka) to produce a preferred range of 9-14 mm/yr (Figure 11) This final slip rate was preferred because 1) both methods of fan reconstruction (as explained in the Offset Models section) yielded exactly 50.0 meters and 2) the mean U-series date (3.5 ka) and the minimum ^{10}Be date (5.4 ka) were proven to be consistent and reliable geochronometers (see section 5.3) for the minimum and maximum Qal3 fan surface depositional ages.

7 Discussion

7.1 Implications for Slip Partitioning in the Coachella Valley

One question that this study attempts to reconcile is whether slip on the Mission Creek strand has stayed constant over Pleistocene to Holocene timescales, and relatedly, whether slip rates are consistent along strike of the fault. We have two slip rate estimates in the Indio Hills for comparison: 1) a Pleistocene slip rate from 5 km to the east at Biskra Palms (Behr et al., 2010) of 12-22 mm/yr (14-17 preferred) and 2) a Holocene to Pleistocene slip rate from 2 km to the west at Pushawalla Canyon (Blisniuk et al., 2013) of 19-25 mm/yr. My slip rate estimate of 7-21 mm/yr overlaps well with the Pleistocene slip rate measured at Biskra Palms, although my preferred rate is slightly slower, but still within error, of the preferred rate there. On the other hand, my rate is just outside the uncertainty bounds of the slip rate estimate at Pushawalla Canyon. Because the Pushawalla Canyon work is in prep for publication, however, the details of that study cannot be investigated at this time; but I

intend to assess the possible sources of differences in these two slip rate estimates for an eventual publication of this thesis work in the near future.

My preferred Holocene right lateral slip rate for the Mission Creek strand of 10-14 mm/yr represents only 50-75% of the slip rate estimated from geodetic block models for SAF strands in the northern Coachella Valley, and 43- 65% of the Indio Strand of the SAF in the southern Coachella Valley (Spinler et al., 2010). This is interesting because it suggests either 1) the present-day rates of the Mission Creek fault have increased over the past several thousand years, 2) the Banning fault is accommodating significant slip at this latitude, and/or 3) there is substantial off-fault deformation within the Indio Hills and surrounding areas that is measured geodetically, but is not incorporated into geologic slip rates estimated from individual structures.

A significant increase of slip rate at this location in the last 0-5 ka seems highly unlikely because my work shows that the rate has stayed consistent from 50 ka (14-17 mm/yr from Behr et al., 2010) to 5 ka (9-14 mm/yr from this study). In order for the Banning fault to be accommodating the remaining 43-75% slip at this latitude, its slip rate would need to be 7-15 mm/yr. However, the geomorphology just 5 km to the east at Biskra Palms Oasis strongly suggests that the Mission Creek fault is the most active strand of the San Andreas fault at this latitude (van der Woerd et al., 2006). Behr et al., (2010), for example, reported an approximate right-lateral Pleistocene geologic slip rate of 1-3 mm/yr for the Banning fault at Biskra Palms. Furthermore, the geomorphology, structure and exhumation of more deeply buried rocks in the northwest Indio Hills suggests the Banning fault slip rate likely peaks in the northwest Indio Hills, and decreases both northwest and southeast of that region (Gold et al., 2015). These arguments suggests that the discrepancy between geodetic and geologic slip rates for the Coachella Valley segment are likely because the geodetic data captures off-fault deformation in the region, whereas the geologic slip rates only incorporate a single fault strand. This is evidenced by the normal faults mapped in the Indio Hills at this latitude (Keller et al., 1982; Behr et al., 2010), as well as the folding of

the Ocotillo Fm observed in this study and in others (Keller et al., 1982). Immediately north of the field area lie the San Bernardino Mountains, which contains the southerwesternmost strands of the Eastern California Shear Zone.

7.2 Implications for Quaternary Dating of Arid Region Alluvial Fans

The age of the Three Palms alluvial fan complex was constrained using two quaternary geochronometers (^{10}Be and U-Series) that yielded a minimum (3.5 +/- 0.92 ka 2σ) and a maximum depositional age (5.4 +/-1.0 ka 95% CI), respectively, and thus bracketed the timing of deposition between 3.5 and 5.4 ka. In addition to constraining the slip rate, these results have some important implications for best practices in acquiring and interpreting Quaternary geochronologic data. Firstly, my work emphasizes the importance of using multiple geochronometers. Many studies have used probability distribution functions of scattered cosmogenic datasets to approximate the depositional age of an alluvial fan, terrace, or other geomorphic feature (Rinterknecht et al., 2005; Putnam et al., 2010; Rodés et al., 2011).

This approach makes the assumption that inheritance, which skews the ages to be older, is perfectly balanced by post-depositional erosional processes that bias the ages too young (Frankel et al., 2007a; Zechar and Frankel, 2009). However, as discussed in Section 5.3, this is highly unlikely to be the case for the Three Palms site as the two chronometers, our field observations, and our data from the modern wash strongly indicate that inheritance dominates the ages in this system. By contrast, there are other sites in southern California that date both Holocene and Pleistocene alluvial fans that had geochronometers that are governed by an erosion dominated system. Behr et al., (2010), for example, observed a systematic correlation between ages and boulder height, suggesting incremental surface lowering through time– the surface lowering effect was larger than a relatively minor effect of inheritance. In Bilsniuk et al, (2012), they collected ^{10}Be and U-series samples from five different Pleistocene and Holocene alluvial fans near the San Jacinto fault. ^{10}Be depth

profiles were constructed for all of these five sites to account for inheritance and to constrain the fan age. All of the inheritance-corrected ^{10}Be dates produced for the three Holocene sites were younger than the U-series ages The two late Pleistocene sites also had a similar issue, but when the effect of erosion was considered, the depth profile model fan ages were in good agreement with the U-series ages. In all of these studies (including my own), robust depositional age estimates were only garnered through combining two geochronometers, whereas without them the age interpretations would have been significantly in error.

The recognition that the Qal3 fan, and the modern catchments nearby are inheritance-dominated may have interesting implications for geomorphic processes in their source catchments. Some explanations for why the Qal3 fan is may be dominated by inheritance rather than a balanced system include 1) the small and steep catchment areas that source the Qal3 fan sediment 2) the thin (less than 1.5 meter) debris flow deposit that was sampled. The Qal3 fan is sourced from a catchment that is very short and has a steep (10°-12°) angle. Although there are rills showing modern wash development and a lightly marked and bar and swale topography, it is obvious that the majority of the boulders that are on the fan surface are not sourced from far away and that they were not transported via these channels. The fact that the boulders on the fan surface do not come from far away implies that the inheritance signal in the fan is dominated by hillslope processes, such as hillslope creep, as opposed to fluvial residence time. Alluvial fan deposition in this area could also be related to wetter climate cycles (Molnar, 2001; Von Blanckenburg, 2005). Interestingly, the depositional age range of the Qal3 fan (5.4-3.5 ka) coincide with the Neopluvial, which was a phase of wetter and colder climates that occurred in the western United States during the late Holocene- between 5.1- 2.5 ka (Madsen, 2000; Hockett, 2015). This scenario would also produce inheritance-dominated clasts, as a debris flow this thin would not have supplied the energy or the distance to mix the catchment and transport buried deposits with low nuclide concentrations.

8 Conclusion

My investigation of a Holocene slip rate site on the Coachella Valley segment of the southern San Andreas fault has demonstrated 1) the Holocene geologic slip rate for the Mission Creek strand is 7-21 mm/yr, with a preferred rate 9-14 mm/yr 2) that this slip on the Mission Creek strand has remained constant from the Pleistocene to the Holocene. This investigation has also strengthened several points that have been explored by previous workers; 1) slip transfer from the Mission Creek to the Banning fault causes a slip rate discrepancy between geologic and geodetic rates because geodetic block models that do not have the resolution to capture slip rates of individual strands and smaller lateral geologic slip rates due to significant off-fault deformation and reverse slip. 2) The use of multiple geochronometers is essential in determining a well constrained geologic slip rate range.

Bibliography

Allen, C. R., 1957: San Andreas fault zone in San Gorgonio Pass,¬¬ southern California. *Geological Society of America Bulletin*, **68(3)**, 315–350.

Amos, C. B., S. J. Brownlee, D. H. Rood, G. B. Fisher, R. Bürgmann, P. R. Renne, and A. S. Jayko, 2013: Chronology of tectonic, geomorphic, and volcanic interactions and the tempo of fault slip near Little Lake, California. *Geological Society of America Bulletin*, **125(7-8)**, 1187–1202.

Anderson, R. S., J. L. Repka, and G. S. Dick, 1996: Explicit treatment of inheritance in dating depositional surfaces using in situ 10Be and 26Al. *Geology*, **24(1)**, 47–51.

Argus, D. F. and R. G. Gordon, 1991: No-net-rotation model of current plate velocities incorporating plate motion model NUVEL-1. *Geophysical research letters*, **18(11)**, 2039–2042.

Armstrong, P. A., R. Perez, L. A. Owen, and R. C. Finkel, 2010: Timing and controls on late Quaternary landscape development along the eastern Sierra El Mayor range front in northern Baja California, Mexico. *Geomorphology*, **114(3)**, 415–430.

Atwater, T., 1970: Implications of plate tectonics for the Cenozoic tectonic evolution of western North America. *Geological Society of America Bulletin*, **81(12)**, 3513–3536.

Becker, T. W., J. L. Hardebeck, and G. Anderson, 2005: Constraints on fault slip rates of the

southern California plate boundary from GPS velocity and stress inversions. *Geophysical Journal International*, **160(2)**, 634–650.

Behr, W., D. Rood, K. Fletcher, N. Guzman, R. Finkel, T. C. Hanks, K. Hudnut, K. Kendrick, J. Platt, W. Sharp, et al., 2010: Uncertainties in slip-rate estimates for the Mission Creek strand of the southern San Andreas fault at Biskra Palms Oasis, southern California. *Geological Society of America Bulletin*, **122(9-10)**, 1360–1377.

Bendick, R., R. Bilham, J. Freymueller, K. Larson, and G. Yin, 2000: Geodetic evidence for a low slip rate in the Altyn Tagh fault system. *Nature*, **404(6773)**, 69.

Bevis, M., K. Hudnut, R. Sanchez, C. Toth, D. Grejner-Brzezinska, E. Kendrick, D. Caccamise, D. Raleigh, H. Zhou, S. Shan, et al., 2005: The B4 project: scanning the San Andreas and San Jacinto fault zones. In *AGU Fall Meeting Abstracts*.

Blisniuk, K., M. Oskin, K. Fletcher, T. Rockwell, and W. Sharp, 2012: Assessing the reliability of U-series and 10 Be dating techniques on alluvial fans in the Anza Borrego Desert, California. *Quaternary Geochronology*, **13**, 26–41.

Blisniuk, K., T. Rockwell, L. A. Owen, M. Oskin, C. Lippincott, M. W. Caffee, and J. Dortch, 2010: Late Quaternary slip rate gradient defined using high-resolution topography and 10Be dating of offset landforms on the southern San Jacinto fault zone, California. *Journal of Geophysical Research: Solid Earth*, **115(B8)**.

Blisniuk, K., K. Scharer, W. Sharp, R. Burgmann, M. Rymer, and P. Williams, 2013: New slip rate estimates for the Mission Creek strand of the San Andreas fault zone. In *AGU Fall Meeting Abstracts*.

Blisniuk, P. M. and W. D. Sharp, 2003: Rates of late Quaternary normal faulting in central Tibet from U-series dating of pedogenic carbonate in displaced fluvial gravel deposits. *Earth and Planetary Science Letters*, **215(1)**, 169–186.

Braucher, R., P. Del Castillo, L. Siame, A. Hidy, and D. Bourles, 2009: Determination of both exposure time and denudation rate from an in situ-produced 10 Be depth profile: a mathematical proof of uniqueness. Model sensitivity and applications to natural cases. *Quaternary Geochronology*, **4(1)**, 56–67.

Capo, R. C. and O. A. Chadwick, 1999: Sources of strontium and calcium in desert soil and calcrete. *Earth and Planetary Science Letters*, **170(1)**, 61–72.

Cheng, H., R. L. Edwards, C.-C. Shen, V. J. Polyak, Y. Asmerom, J. Woodhead, J. Hellstrom, Y. Wang, X. Kong, C. Spötl, et al., 2013: Improvements in 230 Th dating, 230 Th and 234 U half-life values, and U–Th isotopic measurements by multi-collector inductively coupled plasma mass spectrometry. *Earth and Planetary Science Letters*, **371**, 82–91.

Cowgill, E., 2007: Impact of riser reconstructions on estimation of secular variation in rates of strike–slip faulting: Revisiting the Cherchen River site along the Altyn Tagh Fault, NW China. *Earth and Planetary Science Letters*, **254(3)**, 239–255.

Cowgill, E., R. D. Gold, C. Xuanhua, W. Xiao-Feng, J. R. Arrowsmith, and J. Southon, 2009: Low Quaternary slip rate reconciles geodetic and geologic rates along the Altyn Tagh fault, northwestern Tibet. *Geology*, **37(7)**, 647–650.

DeMets, C., R. G. Gordon, and D. F. Argus, 2010: Geologically current plate motions. *Geophysical Journal International*, **181(1)**, 1–80.

Densmore, A. L., M. A. Ellis, Y. Li, R. Zhou, G. S. Hancock, and N. Richardson, 2007: Active tectonics of the Beichuan and Pengguan faults at the eastern margin of the Tibetan Plateau. *Tectonics*, **26(4)**.

Dibblee, T. W., 1964: *Geologic map of the San Gorgonio Mountain quadrangle, San Bernardino and Riverside Counties, California*. US Geological Survey.

—, 1967: *Geologic map of the Morongo Valley quadrangle, San Bernardino and Riverside Counties, California*. US Geological Survey.

Dorsey, R. J., 2003: Late Pleistocene slip rate on the Coachella Valley segment of the San Andreas Fault and implications for regional slip partitioning. In *Geol. Soc. Am. Abstr. Prog*, vol. 35.

Dunai, T. J., 2010: *Cosmogenic Nuclides: Principles, concepts and applications in the Earth surface sciences*. Cambridge University Press.

Fay, N. P. and E. D. Humphreys, 2005: Fault slip rates, effects of elastic heterogeneity on geodetic data, and the strength of the lower crust in the Salton Trough region, southern California. *Journal of Geophysical Research: Solid Earth*, **110(B9)**.

Fialko, Y., 2006: Interseismic strain accumulation and the earthquake potential on the southern San Andreas fault system. *Nature*, **441(7096)**, 968.

Field, E. H., 2007: A summary of previous working groups on California earthquake probabilities. *Bulletin of the Seismological Society of America*, **97(4)**, 1033–1053.

Fletcher, K. E., W. D. Sharp, K. J. Kendrick, W. M. Behr, K. W. Hudnut, and T. C. Hanks, 2010: 230Th/U dating of a late Pleistocene alluvial fan along the southern San Andreas fault. *Geological Society of America Bulletin*, B30018–1.

Frankel, K. L., K. S. Brantley, J. F. Dolan, R. C. Finkel, R. E. Klinger, J. R. Knott, M. N. Machette, L. A. Owen, F. M. Phillips, J. L. Slate, et al., 2007a: Cosmogenic 10Be and 36Cl geochronology of offset alluvial fans along the northern Death Valley fault zone: Implications for transient strain in the eastern California shear zone. *Journal of Geophysical Research: Solid Earth*, **112(B6)**.

Frankel, K. L., J. F. Dolan, R. C. Finkel, L. A. Owen, and J. S. Hoeft, 2007b: Spatial variations in slip rate along the Death Valley-Fish Lake Valley fault system determined from

LiDAR topographic data and cosmogenic 10Be geochronology. *Geophysical Research Letters*, **34(18)**.

Fryer, R. C., 2016: Holocene Geologic Slip Rate for Mission Creek Strand of the southern San Andreas fault. *Thesis*.

Fumal, T., M. Rymer, and G. Seitz, 2002: Timing of large earthquakes since AD 800 on the Mission Creek strand of the San Andreas fault zone at Thousand Palms Oasis, near Palm Springs, California. *Bulletin of the Seismological Society of America*, **92(7)**, 2841–2860.

Gile, L. H., F. F. Peterson, and R. B. Grossman, 1965: The K Horizon: A Master Soil Horizons of Carbonate Accumulations. *Soil Science*, **99(2)**, 74–82.

Gold, P. and W. Behr, 2016: Review of Published Quaternary Geochronologic Data Supports the Importance of Dating Geomorphic Surfaces Using Multiple Geochronometers. In *AGU Fall Meeting Abstracts*.

Gold, P. O., W. M. Behr, D. Rood, W. D. Sharp, T. K. Rockwell, K. Kendrick, and A. Salin, 2015: Holocene geologic slip rate for the Banning strand of the southern San Andreas Fault, southern California. *Journal of Geophysical Research: Solid Earth*, **120(8)**, 5639–5663.

Gosse, J., E. McDonald, and R. Finkel, 2003: Cosmogenic nuclide dating of arid region alluvial fans. In *Geological Society of America Abstracts with Programs*, vol. 35, p. 8.

Gosse, J. C. and F. M. Phillips, 2001: Terrestrial in situ cosmogenic nuclides: theory and application. *Quaternary Science Reviews*, **20(14)**, 1475–1560.

Gutenberg, B., 1941: Mechanism of faulting in southern California indicated by seismograms. *Bulletin of the Seismological Society of America*, **31(4)**, 263–302.

Heermance, R. V. and J. D. Yule, 2015: Holocene slip rates along the San Andreas Fault

System in the San Gorgonio Pass and implications for large earthquakes in southern California. *Geophysical Research Letters*.

Hidy, A. J., J. C. Gosse, J. L. Pederson, J. P. Mattern, and R. C. Finkel, 2010: A geologically constrained Monte Carlo approach to modeling exposure ages from profiles of cosmogenic nuclides: An example from Lees Ferry, Arizona. *Geochemistry, Geophysics, Geosystems*, **11(9)**.

Hill, M. L. and T. W. Dibblee, 1953: San Andreas, Garlock, and Big Pine faults, California a study of the character, history, and tectonic significance of their displacements. *Geological Society of America Bulletin*, **64(4)**, 443–458.

Hockett, B., 2015: The zooarchaeology of Bonneville Estates Rockshelter: 13,000 years of Great Basin hunting strategies. *Journal of Archaeological Science: Reports*, **2**, 291–301.

Jaffey, A., K. Flynn, L. Glendenin, W. t. Bentley, and A. Essling, 1971: Precision measurement of half-lives and specific activities of U 235 and U 238. *Physical Review C*, **4(5)**, 1889.

Keller, E., M. Bonkowski, R. Korsch, and R. Shlemon, 1982: Tectonic geomorphology of the San Andreas fault zone in the southern Indio Hills, Coachella Valley, California. *Geological Society of America Bulletin*, **93(1)**, 46–56.

Kendrick, K. J., J. Matti, and S. Mahan, 2015: Late Quaternary slip history of the Mill Creek strand of the San Andreas fault in San Gorgonio Pass, southern California: The role of a subsidiary left-lateral fault in strand switching. *Geological Society of America Bulletin*, **127(5-6)**, 825–849.

Kirby, E., D. W. Burbank, M. Reheis, and F. Phillips, 2006: Temporal variations in slip rate of the White Mountain fault zone, eastern California. *Earth and Planetary Science Letters*, **248(1)**, 168–185.

Lal, D., 1991: Cosmic ray labeling of erosion surfaces: in situ nuclide production rates and erosion models. *Earth and Planetary Science Letters*, **104(2-4)**, 424–439.

Langbein, J., R. Borcherdt, D. Dreger, J. Fletcher, J. L. Hardebeck, M. Hellweg, C. Ji, M. Johnston, J. R. Murray, R. Nadeau, et al., 2005: Preliminary report on the 28 September 2004, M 6.0 Parkfield, California earthquake. *Seismological Research Letters*, **76(1)**, 10–26.

Lawson, A. C. and H. F. Reid, 1908: *The California Earthquake of April 18, 1906: Report of the State Earthquake Investigation Commission....* No. 87, Carnegie institution of Washington.

Lindsey, E. and Y. Fialko, 2013: Geodetic slip rates in the southern San Andreas Fault system: Effects of elastic heterogeneity and fault geometry. *Journal of Geophysical Research: Solid Earth*, **118(2)**, 689–697.

Machette, M. N., 1985: Calcic soils of the southwestern United States. *Geological Society of America Special Papers*, **203**, 1–22.

Madsen, D. B., 2000: *Late quaternary paleoecology in the Bonneville Basin*. No. 130, Utah Geological Survey.

Matti, J. C. and D. M. Morton, 1993: Paleogeographic evolution of the San Andreas fault in southern California: A reconstruction based on a new cross-fault correlation. *Geological Society of America Memoirs*, **178**, 107–160.

Matti, J. C., D. M. Morton, and B. F. Cox, 1992: The San Andreas fault system in the vicinity of the central Transverse Ranges province, southern California. Tech. rep., US Geological Survey,.

Mayer, L., L. D. McFadden, and J. W. Harden, 1988: Distribution of calcium carbonate in desert soils: A model. *Geology*, **16(4)**, 303–306.

McDonald, E. V., F. B. Pierson, G. N. Flerchinger, and L. D. McFadden, 1996: Application of a soil-water balance model to evaluate the influence of Holocene climate change on calcic soils, Mojave Desert, California, USA. *Geoderma*, **74(3-4)**, 167–192.

Minster, J. B. and T. H. Jordan, 1978: Present-day plate motions. *Journal of Geophysical Research: Solid Earth*, **83(B11)**, 5331–5354.

Molnar, P., 2001: Climate change, flooding in arid environments, and erosion rates. *Geology*, **29(12)**, 1071–1074.

Morris, J. D., 1991: Applications of Cosmogenic be to Problems in the Earth Sciences. *Annual Review of Earth and Planetary Sciences*, **19(1)**, 313–350.

Oskin, M., L. Perg, D. Blumentritt, S. Mukhopadhyay, and A. Iriondo, 2007: Slip rate of the Calico fault: Implications for geologic versus geodetic rate discrepancy in the eastern California shear zone. *Journal of Geophysical Research: Solid Earth*, **112(B3)**.

Owen, L. A., S. J. Clemmens, R. C. Finkel, and H. Gray, 2014: Late Quaternary alluvial fans at the eastern end of the San Bernardino Mountains, Southern California. *Quaternary Science Reviews*, **87**, 114–134.

Owen, L. A., K. L. Frankel, J. R. Knott, S. Reynhout, R. C. Finkel, J. F. Dolan, and J. Lee, 2011: Beryllium-10 terrestrial cosmogenic nuclide surface exposure dating of Quaternary landforms in Death Valley. *Geomorphology*, **125(4)**, 541–557.

Phillips, W. M., E. V. McDonald, S. L. Reneau, and J. Poths, 1998: Dating soils and alluvium with cosmogenic 21 Ne depth profiles: case studies from the Pajarito Plateau, New Mexico, USA. *Earth and Planetary Science Letters*, **160(1)**, 209–223.

Putnam, A., J. Schaefer, D. Barrell, M. Vandergoes, G. Denton, M. Kaplan, R. Finkel, R. Schwartz, B. Goehring, and S. Kelley, 2010: In situ cosmogenic 10 Be production-rate calibration from the Southern Alps, New Zealand. *Quaternary Geochronology*, **5(4)**, 392–409.

Repka, J. L., R. S. Anderson, and R. C. Finkel, 1997: Cosmogenic dating of fluvial terraces, Fremont River, Utah. *Earth and Planetary Science Letters*, **152(1)**, 59–73.

Rinterknecht, V. R., L. Marks, J. A. Piotrowski, G. M. RAISBECK, F. Yiou, E. J. BROOK, and P. U. CLARK, 2005: Cosmogenic 10 Be ages on the pomeranian moraine, Poland. *Boreas*, **34(2)**, 186–191.

Rodés, Á., R. Pallàs, R. Braucher, X. Moreno, E. Masana, and D. L. Bourlés, 2011: Effect of density uncertainties in cosmogenic 10 Be depth-profiles: dating a cemented Pleistocene alluvial fan (Carboneras Fault, SE Iberia). *Quaternary Geochronology*, **6(2)**, 186–194.

Sauber, J., W. Thatcher, S. C. Solomon, and M. Lisowski, 1994: Geodetic slip rate for the eastern California shear zone and the recurrence time of Mojave Desert earthquakes. *Nature*, **367(6460)**, 264–266.

Schwarcz, H. and A. Latham, 1989: Dirty calcites 1. Uranium-series dating of contaminated calcite using leachates alone. *Chemical Geology: Isotope Geoscience section*, **80(1)**, 35–43.

Schwarcz, H. P., 1989: Uranium series dating of Quaternary deposits. *Quaternary International*, **1**, 7–17.

Schwartz, D., D. Pantosti, K. Okumura, T. Powers, and J. Hamilton, 1998: Paleoseismic investigations in the Santa Cruz mountains, California: Implications for recurrence of large-magnitude earthquakes on the San Andreas Fault. *Journal of Geophysical Research: Solid Earth*, **103(B8)**, 17985–18001.

Senftle, F., T. Farley, and N. Lazar, 1956: Half-life of Th 232 and the branching ratio of Bi 212. *Physical Review*, **104(6)**, 1629.

Sharp, W. D., K. R. Ludwig, O. A. Chadwick, R. Amundson, and L. L. Glaser, 2003: Dating fluvial terraces by 230 Th/U on pedogenic carbonate, Wind River Basin, Wyoming. *Quaternary Research*, **59(2)**, 139–150.

Sieh, K., 1986: Slip rate across the San Andreas fault and prehistoric earthquakes at Indio, California. *Eos Trans. AGU*, **67(44)**, 1200.

Sieh, K., M. Stuiver, and D. Brillinger, 1989: A more precise chronology of earthquakes produced by the San Andreas fault in southern California. *Journal of Geophysical Research: Solid Earth*, **94(B1)**, 603–623.

Sieh, K. E. and P. L. Williams, 1990: Behavior of the southernmost San Andreas fault during the past 300 years. *Journal of Geophysical Research: Solid Earth*, **95(B5)**, 6629–6645.

Sigloch, K. and M. G. Mihalynuk, 2013: Intra-oceanic subduction shaped the assembly of Cordilleran North America. *Nature*, **496(7443)**, 50.

Spinler, J. C., R. A. Bennett, M. L. Anderson, S. F. McGill, S. Hreinsdóttir, and A. McCallister, 2010: Present-day strain accumulation and slip rates associated with southern San Andreas and eastern California shear zone faults. *Journal of Geophysical Research: Solid Earth*, **115(B11)**.

van der Woerd, J., Y. Klinger, K. Sieh, P. Tapponnier, F. J. Ryerson, and A.-S. Mériaux, 2006: Long-term slip rate of the southern San Andreas fault from 10Be-26Al surface exposure dating of an offset alluvial fan. *Journal of Geophysical Research: Solid Earth*, **111(B4)**.

Von Blanckenburg, F., 2005: The control mechanisms of erosion and weathering at basin scale from cosmogenic nuclides in river sediment. *Earth and Planetary Science Letters*, **237(3)**, 462–479.

Wallace, R. E., 1970: Earthquake recurrence intervals on the San Andreas fault. *Geological Society of America Bulletin*, **81(10)**, 2875–2890.

Weldon, R. J. and K. E. Sieh, 1985: Holocene rate of slip and tentative recurrence interval

for large earthquakes on the San Andreas fault, Cajon Pass, southern California. *Geological Society of America Bulletin*, **96(6)**, 793–812.

Wesnousky, S. G., C. S. Prentice, and K. E. Sieh, 1991: An offset Holocene stream channel and the rate of slip along the northern reach of the San Jacinto fault zone, San Bernardino Valley, California. *Geological Society of America Bulletin*, **103(5)**, 700–709.

Willis, B., 1938: San Andreas Rift, California. *The Journal of Geology*, **46(6)**, 793–827.

Yule, D. and K. Sieh, 2001: The paleoseismic record at Burro Flats: Evidence for a 300-year average recurrence for large earthquakes on the San Andreas fault in San Gorgonio Pass, southern California. In *Geol. Soc. Am. Abs. Programs—Cordilleran Section Meeting (April)*, vol. 33, p. 31.

—, 2003: Complexities of the San Andreas fault near San Gorgonio Pass: Implications for large earthquakes. *Journal of Geophysical Research: Solid Earth*, **108(B11)**.

Zechar, J. D. and K. L. Frankel, 2009: Incorporating and reporting uncertainties in fault slip rates. *Journal of Geophysical Research: Solid Earth*, **114(B12)**.

Zielke, O., J. R. Arrowsmith, L. G. Ludwig, and S. O. Akçiz, 2010: Slip in the 1857 and earlier large earthquakes along the Carrizo Plain, San Andreas fault. *Science*, **327(5969)**, 1119–1122.

Vita

Juan Jose (JJ) Munoz was born on the western flank of the central Andean Cordillera in Manizales, Colombia, which at an elevation of 7500' and a tropical latitude, experiences absurdly beautiful weather and overlooks acres of coffee fields and the powerful Nevado del Ruiz volcano. Unfortunately, (but fortunately) for him, his family relocated to Phoenix, Arizona- a city that is a testament to the stubbornness of mankind, when he was 2 years old in search of a better life in his adoptive country. The love of our natal planet and its processes was introduced to him early on by his parents, both earth scientists in their own right. This led him to pursue degrees in Geology and Environmental Studies at the University of Arizona in 2011, graduating in 2015. Immediately thereafter, his interest in Structural Geology led him to the University of Texas at Austin to pursue and complete an M.S. degree in Geology. However, an even greater interest in the societal implications of earth sciences and a rekindling of his degree in Environmental Studies has led him to the Texas Commission on Environmental Quality, where he will be working in the State Superfund section of the agency. When not curtailing his lifespan by hanging out on viciously contaminated sites for work, you can find JJ singing an obnoxious Carlos Vives song at the top of his lungs while driving Garnet, his precious 2005 Ford Escape. Or perhaps you can catch him and Patrick Boyd, "double bacon cheeseburgers" in hand, catching a soccer game at the Crown.

1941 E. Clubhouse Dr. Phoenix, AZ, 85048

This dissertation was typeset with LaTeX 2ε[1] by the author.

[1] LaTeX 2ε is an extension of LaTeX. LaTeX is a collection of macros for TeX. TeX is a trademark of the American Mathematical Society. The macros used in formatting this dissertation were written by Dinesh Das, Department of Computer Sciences, The University of Texas at Austin, and extended by Bert Kay, James A. Bednar, and Ayman El-Khashab.